A Thesis

Entitled

The Effects of Ball Burnishing for Aerospace Blade Material 17-4 PH Steel

By

Tao Zhang

Submitted to the Graduate Faculty as partial fulfillment of the requirements for

The Master of Science Degree in

Mechanical Engineering

____

Dr. Ioan D. Marinescu, Committee Chair

____

Dr. Abdollah Afjeh, Committee Member

____

Dr. Hongyan Zhang, Committee Member

____

Dr. Patricia R. Komuniecki, Dean

College of Graduate Studies

The University of Toledo

December 2013

An Abstract of

The Effects of Ball Burnishing for Aerospace Blade Material 17-4 PH Steel

By

Tao Zhang

Submitted to the Graduate Faculty as partial fulfillment of the requirements for
The Master of Science Degree in
Mechanical Engineering

The University of Toledo

December 2013

Ball burnishing has been investigated to improve surface integrity which directly affects component's quality and performance. Examination of many serious accidents involving aeroengines, has revealed that failure of the first stage compressor blades impacted by foreign object damage (FOD) was the main reason caused, such as bird strikes. Aerospace material 17-4 PH stainless steel with its high mechanical properties is used for the first stage compressor blades of aeroengine to reduce failure from FOD; however, the effects of burnishing on surface integrity of 17-4 PH steel have not been well documented.

In this research, it is demonstrated that improvement is material properties can be achieved by hydrostatic ball burnishing applied to 17-4 PH steel, such as smoother surfaces, enhanced surface hardness and impact strength, and high magnitude of compressive residual stresses with a greater depth of layer. For surface roughness, burnishing pressure, speed and feed are significant factors whereas turned surface roughness is negligible. A second-order empirical model was obtained and validated with experimental data. The pressure is the most important factor for both surface hardness and impact strength, as well as for residual stresses at the surface and maximum magnitude with its depth. The triaxial residual stress profiles were obtained while the hook-shaped residual stress profiles were observed under low pressure. The full width at half maximum (FWHM) values show the near-surface work hardening state as one evidence assisted with the analysis of surface hardness and impact strength. The results indicated the potential benefits of the ball burnishing application for the aerospace blade material.

Acknowledgements

First of all, I would like to thank my advisor, Professor Ioan D. Marinescu, for his support, guidance, and encouragement throughout my study at the University of Toledo.

I am very thankful to the MIME department faculty and staff for their help and understanding. Special thanks to Professor and Chairman Abdollah Afjeh and Dr. Hongyan Zhang for serving on my committee.

I would like to show my gratitude to Mr. John Jaegly and Tim Grivanos of MIME machine shop staff and Mr. Todd Gearig of Master Chemical Corp. for the help of machining and burnishing processes.

In particular, I am greatly thankful to the Instrumentation Center staff Dr. Pannee Burckel and Dr. Kristin Kirschbaum for the instruction of X-ray diffraction.

I would also like to thank Mr. Matt Van Acker of Able Electropolishing Co. Inc. and Ms. Nancy Zapata of Control Electropolishing Corp. for the help of electropolishing.

I am extremely grateful to my friends, especially Dr. Nilo T. Bugtai in Precision Micro-Machining Center for the help of useful advices.

Finally, I would like to thank my wife for her support, patience and encouragement.

Table of Contents

List of Tables

List of Figures

List of Symbols

Ra……………….Algorithmic surface roughness
RaB……………..Surface roughness Ra by burnishing
RaT……………..Surface roughness Ra by turning

P……………. ….Burnishing pressure
S………………...Burnishing surface speed
F………………...Burnishing feed rate

$\sigma_\theta(r_i)$……………True circumferential stress at radius r_i
$\sigma_\theta^m(r_i)$…………..Measured circumferential stresses at radius r_i
$\sigma_r(r_i)$……………True radial stress at radius r_i
$\sigma_z(r_i)$……………True axial stresses at radius r_i
$\sigma_z^m(r_i)$…………..Measured axial stresses at radius r_i

Chapter 1

Introduction

1.1 Overview

Surface enhancement is well known as one of the most important methods to improve product performance by improving surface properties, such as surface hardening, which can be traced back to thousands of years. Surface enhancement techniques, such as thermal, thermochemical, and mechanical techniques, have prospered greatly since the early twentieth century [1].

The studies of mechanical surface treatments increasingly focused on surface and subsurface characteristics in industrial fields, such as shot peening (SP), ultrasonic shot peening (USP), and ball-burnishing (BB) which induced the highest and deepest maximum residual stress [2]. As a quite sufficient mechanical process in applications of dynamic loading [3], modern burnishing was applied in the early part of last century in the U.S., in which the history may need to be verified for some different introductions in literatures. Altenberger [1] introduced this burnishing process which was carried out in the U.S. on the axes of Ford T vehicle in the 1920s and later on the axes of trains in the 1930s. However, the recent researches reported by Luca [4] and Sorin [5] indicated that it was introduced in the United States in the 50s of the last century after it was applied first in Germany in the twenties of the last century and then USSR.

Burnishing is a cold work that employs plastic deformation of a surface layer in order to improve surface characteristics, such as surface finish and hardness of a workpiece [4]. As a no chip process in the environmental benefit, it is essentially a forming operation that occurs on a small scale in which strain hardening is induced to improve the surface strength and hardness with mirror like surface finish and high compressive residual stress in the surface layer, resulting in better fatigue life [6].

The plastic deformation produced by roller or ball burnishing is a displacement of the material in which the tool pushes the materials at the surface from the peaks into the valleys under the normal force against the surface over the yield point of materials in Figure 1-1 [6]. The compressive residual stresses induced in the surface layer enhance fatigue performance and mitigate stress corrosion cracking (SCC). In contrast, the tensile stresses reduce fatigue life and tend to surface cracking [7]. The tensile stresses can be generated from the previous machining processes, such as turning, grinding. Some researches show that low plasticity burnishing (LPB) induces deep compressive residual stresses with several benefits of mitigating fatigue damages including foreign objective damage (FOD), fretting, and SCC [8]. Moreover, burnishing process also transforms tensile residual stresses into compressive residual stresses in the surface zone. Under certain conditions, it provides a manufacturing alternative to grinding, precision turning, and honing operations [9] with a cheaper cost which is shown in a previous work on burnishing that only for surface finish there was about 8-15 times less expensive than grinding [4]. Burnishing is widely used on various materials such as steels [7, 10, 11, 12, 13, 14, 15, 16], aluminum alloys [17, 18], titanium alloys [2, 19], magnesium alloys [20, 21, 22], cobalt-chromium alloy [23], and brass [24]. The applications involve about soft materials and hard materials (up to 65 HRC) in manufacturing automotive crankshafts, inner and outer bearing races, bogies axles, etc. [4, 10]. In recent years, the burnishing process is employed increasingly to the aerospace, medical, and nuclear industries [25].

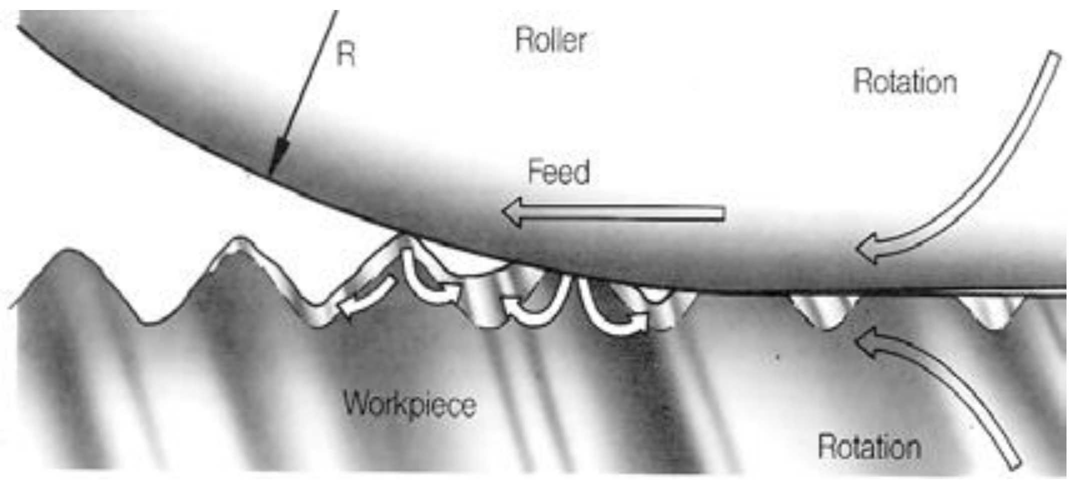

Figure 1-1 Plastic deformation by burnishing [26].

1.2 Burnishing types

A burnishing tool clamped in the conventional or CNC machine can work similarly as the turning process for cylindrical workpiece in a lathe or for flat workpiece in a milling machine, in which the parameter can be set up usually depending on properties of workpiece, such as hardness, and the objectives of works such as surface roughness and residual stress [11, 27]. Based on the tip movement related to the tool holder, burnishing can be simply classified into three basic types including roller, ball and slide burnishing processes. In views of burnishing tool motion with the frequency of oscillation, three types of burnishing can be achieved, namely, vibratory, sonic, and ultrasonic burnishing due to the magnitude of frequency, which can be considered as additional processes, e.g., Loh et al. [28] sorted ball burnishing into three types including normal, vibratory and ultrasonic ball burnishing processes. The burnishing tool oscillatory moves perpendicular to rotation direction (usually oscillatory feed), combined to other normal processes, such as vibratory ball burnishing, thereby increasing the number of control parameters to get additional advantages such as production of controlled surface microgeometry, good contact stiffness, better oil retention capacity, low friction and wear compared with normal burnishing processes [29]. Alternative to grinding, vibratory ball burnishing led to a significant increase of surface oil retentiveness which was achieved in the application of a ship's shaft [30] and high improvement in the longevity of deposition of solid lubricant films [31].

By combining the burnishing process with other processes, some new hybrid types were created, e.g., Laser-assisted burnishing (LAB) which employed a laser beam just ahead of a burnishing tool in order to soften hard materials for burnishing [12], cryogenic burnishing for studies in grain size refinement and phase transformation by cooling the burnished area [23].

Compared to slide burnishing with the pure sliding motion, roller and ball burnishing processes are rolling types which are the most popular due to their simplicity, great techniques, and economic advantages for decades [6]. It should be noticed that in Europe roller burnishing can use either a roller or a ball as the burnishing tool and usually focus on creation of low roughness with lower forces or pressure, in comparison with deep rolling which induces deep compressive residual stresses by using rollers or balls [1, 32].

1.2.1 Roller burnishing

In roller burnishing, a roller or rollers are forced in rotation or planetary rotation over a machined surface seen in Figure 1-2 in which the roller keeps an angle α avoiding over-burnished [26]. Roller burnishing tools are basically classified into two groups, single roller tools and multi-roller tools. Single roller tools are designed for variously irregular surfaces, such as contours, fillets, and grooves as well as cylindrical and tapered external surfaces and bores [26]. According to force control method, the single roller tools also can be classified into mechanical and hydrostatic tools [9]. Multi-roller burnishing tools resemble roller bearings, but the rollers are generally slightly tapered so that their envelope diameter can be accurately adjusted for internal and external cylindrical surfaces. A combined skive-burnishing tool for hydraulic and pneumatic cylinders is made so that multi rollers are combined behind a multi-point cutting tool for machining cylinder inner surfaces [26].

The influences of process parameters on surface characteristics, such as surface roughness and hardness, have been investigated for metals, e.g., EN Series steels, Aluminum alloys and Alpha-beta brass [18]. El-Tayeb et al. [18] applied roller burnishing process to Aluminum 6061 in different burnishing orientations and the results showed that an increase in the roller contact width led to less improvement in the surface roughness, and a 46% reduction in the friction coefficient was obtained when sliding took place in the direction parallel to feed direction. The results indicate that rolling action should be obtained at contact surface in a higher rate direction at speed compared to feed rate in order to minimize the effects of friction on surface quality, which might be the reason why the applications of roller burnishing have not been conducted on another different direction [33].

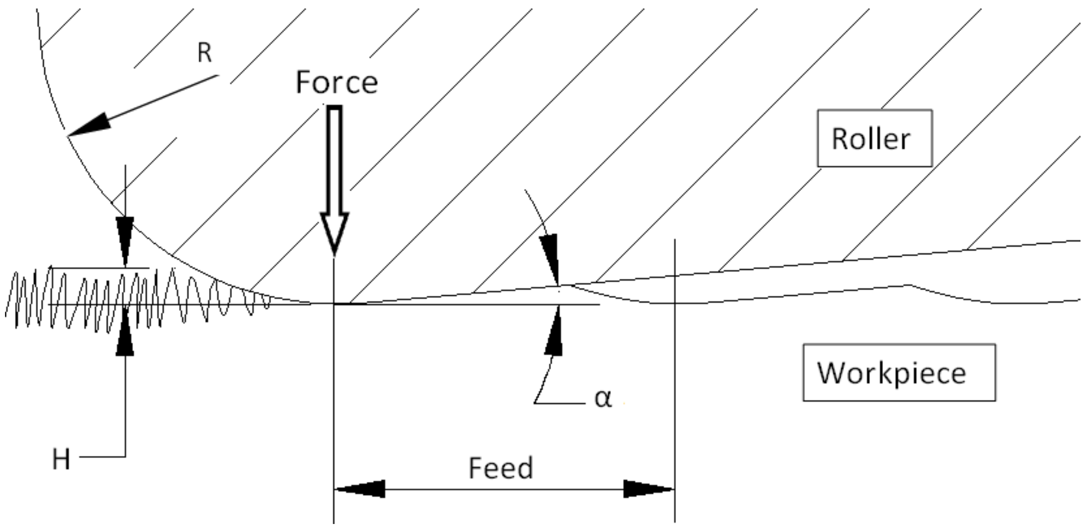

Figure 1-2 Surface geometry for roller burnishing [26].

1.2.2 Ball burnishing

Ball burnishing with its characteristics of free rotation has two types, mechanical and hydrostatic springs, used in the industry [13]. Recent literatures showed several innovations published for mechanical spring ball burnishing tools, such as a self-lubricating polymer bearing [34], a load cell to directly determine and monitor the burnishing force [11], a tool with four single-ball-burnishing tools for large flat surfaces [17], and center rest equipped with three burnishing balls [35], in which a very low surface finish equivalent to polishing was achieved by using a special design tool equipped with a 7 mm ball and three-roller bearing seat [36]. The mechanical spring tool is simple and easy to use just like turning tools or mill cutters; however, the main disadvantage of mechanical spring is obvious for the need of spring adjustment or changing following the load variation [10, 13].

In contrast, the main advantages of hydrostatic spring include a constant load (pressure easily adjusted), hydrostatic film kept between the ball and bearing seat, and overflow fluid to lubricate the workpiece [10], which makes the hydrostatic tool little wearing and is suitable for manufacturing and also is employed in the overwhelming majority of literatures. For hard materials (over 45 HRC), a literature [4] indicated a single-point burnishing tool as the most effective due to reasonable normal forces, resulting from a small contact area. LPB developed by Lambda (Figure 1-3) is very similar to deep rolling even though between them there are some differences among which mainly the difference is LPB generates much less amount of cold work. In addition, the burnishing force is not only limited to a constant during the whole process but also can be adjusted by changing parameters such as pressure to apply a smooth gradient of residual stress for applications [37].

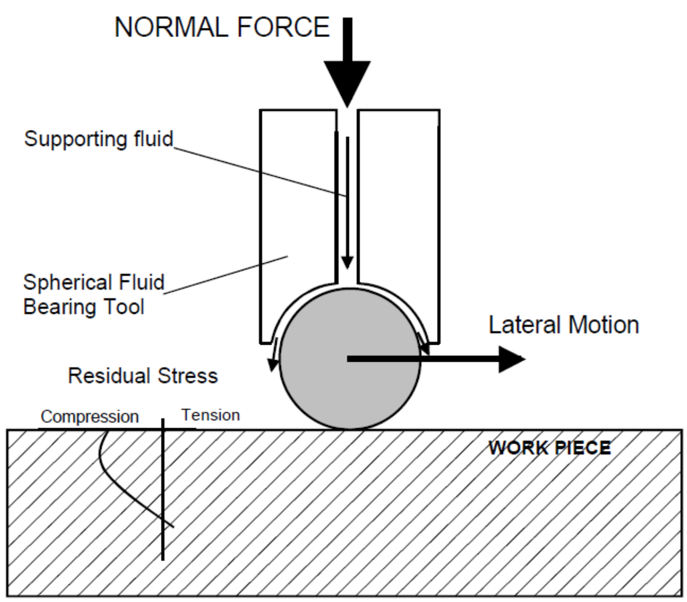

Figure 1-3 Schematic of LPB [37].

1.2.3 Slide burnishing

In slide burnishing, the tip of the tool is fixed to slide purely over the workpiece with significant friction forces in both directions which may cause two drawbacks including rapid tool wear and particular scaly surface [38]. Some studies showed that slide burnishing with cylindrical tools was more productive than that with ball-shaped tools in which very similar values of surface roughness Ra were obtained [11, 39].

Slide burnishing tool is made of diamond due to its high hardness, abrasion resistance and low metal slide friction coefficient. Nevertheless, until now it is impossible to make large-scale diamond tools and slide burnishing tool often employs ball-shaped endings. As a comparison, a study by using a cylinder-shaped tool made of Ti_3SiC_2 base diamond composite achieved similar effects to that of the ball-shaped tool on the improvement of surface layer and fatigue life [39]. The spherical motion burnishing tool is designed for external cylindrical surfaces and relatively long workpieces, in which the motion is along a combination of spherical motion and rectilinear motion with a certain angle of axes [40]. A special tool was designed by Pa [41] for continuous finishing processes combined with burnishing and electrochemical processes. This tool included an annular form electrode and a burnishing tool and was effectively executed on a bore surface finish with direct current (DC) power supply, electrolytic, etc. The result showed that small end radius or thickness of the electrode led to its finish advantage of more sufficient discharge and high speed of tool rotation gave a better finishing. A tool for eccentric burnishing to make oil pockets of slide-bearing sleeves in the internal surfaces was employed by Korzynski [42]. In this study, the tool was designed as a slide burnishing method, and it was mounted on a rotated spindle which was parallel to the workpiece but not coincided on the axis so that it only burnished a portion of the internal surfaces to achieve desirable pits (oil pockets) to collect lubricant as well as dirt and wear products.

1.3 Aerospace compressor blade materials

Modern jet aircrafts are fast and relatively quiet based on high reliability of aeroengine in service [43], in which the aerospace compressor blades work in critical conditions, and the materials have good ductility, high strength at high temperature, and good corrosion resistance. The failure of compressor blades is one of the common situations for compromising the safety. The first stage compressor blades are so important that many serious accidents involving aeroengine indicated that the failure of the first stage compressor blades was the main reason for foreign object damage (FOD) [44], such as impacts of sands and birds. The recent report shows that bird and other wildlife strikes cost over $700 million per year in damage to U.S. civil and military aviation [45]. The root causes of the failure of high compressor blades were focused on FOD with a significant effect on fatigue life even though no sudden fracture happened [46].

Aluminum and titanium based light alloys are commonly used for compressor blades to reduce the weight [43]. The first five to eight stages of compressor blades are made from martensitic high temperature stainless steel (like GTD-450) or 15-5 PH [47]. Moreover, for the defense against ingested debris, some applications involved the first stage compressor blades in use of high strength stainless steel alloys [43]. Precipitation hardened martensitic stainless steels (like 17-4 PH) are widely employed for high strength and high corrosion resistance [48]. With its good combination of high strength, toughness, wear and corrosion resistance [49], 17-4 PH steel was employed in the T56 turboprop engine as the 1st stage compressor blade material [50]. Compared to Alloy 450, 17-4 PH appeared to have lightly better results in high cycle fatigue (HCF) test and stress corrosion cracking (SCC) by LPB [51].

1.4 Objectives of research

Some studies [7, 48, 50, 51] showed that ball burnishing applied to compressor blades highly improved fatigue life, especially the first stage blades. However, the effects of burnishing on surface integrity of 17-4 PH steel have not been well documented. In this research, the major objective based on experimental analysis aims to 1) investigate the influence of ball burnishing parameters on surface integrity, such as surface roughness, hardness, and residual stresses; 2) obtain the empirical model of surface roughness; 3) try to find the optimal compressive residual stress profiles assisted with impact strength results.

In this thesis, the following Chapter 2 shows literature reviews on effects of ball burnishing on surface integrity such as surface roughness, hardness, and residual stress.

Chapter 3 provides the descriptions of the experimental procedures including design of ball burnishing process for 17-4 PH steel bars, workpiece preparation for measurements as well as for Charpy V-notch impact tests due to the possibility that impact from large debris like birds and increased aircraft speeds. Surface roughness, hardness, and residual stresses are considered as the surface integrity factors.

Chapter 4 presents the experimental results and discussions on the surface integrity resulting from burnishing experiments. The effects of process parameters are obtained on surface roughness, hardness, impact strength, and residual stresses. The analyses of surface hardness and impact strength are assisted with the FWHM values. An empirical model is obtained to predict the surface roughness. Other predictive models on residual stresses are to describe the relationship between residual stresses and parameters. Triaxial residual stresses profiles are also established by following the impact results.

In Chapter 5, a summary of conclusions are made from this work as well as recommendation for future work.

Chapter 2

Literature review

2.1 Introduction of plastic deformation

It is well known that plastic deformation in crystals occurs by dislocation slips [52, 53]. A dislocation, namely a linear crystal imperfection, was proposed independently by Orowan, Polanyi, and Taylor in 1934, generally with part edge and part screw dislocation [53]. Almost all the metals are polycrystalline [54]. In the early stages of plastic deformation, work hardening or strain hardening by the increase of stress with plastic deformation is mainly induced by dislocation pile-up due to stuck dislocations across a grain through a narrow transition zone or grain boundary as an effective slip barrier. The dislocation interactions then appear as the increase of dislocation density which is responsible for a higher hardening rate always in a polycrystalline metal than in a single crystal, so yield strength controlled by dislocation interactions only exists in the later stages of deformation [52]. Altenberger [1] introduced that deep rolling could result in the microstructures with dislocation cell structures, nanocrystallites, twinning, or phase transformations. Due to the bcc crystal lattice in 17-4 PH steel, it can be suggested that dislocation cell structures are preferred after ball burnishing.

2.2 Ball burnishing on surface integrity

Recently, many investigations about the burnishing processes were focused on ball burnishing process which could be due to its advantages [4, 10, 14]. Figure 2-1 shows the surface characteristic during ball burnishing process. In addition, an increasing tendency for machining hard steels is to employ ball burnishing as the finish process [55]. Manajan et al. [56] reported that most studies involving ball burnishing focused on effects of process parameters, mainly pressure (force), speed, and feed, followed by number of passes, ball diameter, lubricant, etc., on surface integrity. For hydrostatic ball burnishing, due to pressurized fluid over the tip of tool and workpiece surface with its lubricating and cooling functions, temperature is not considered to rise up to generate the change of microstructure such as recrystallization, grain growth, and phase transformation [57], thus studies may mainly concentrate on other aspects of surface integrity, such as surface roughness, hardness, and residual stresses.

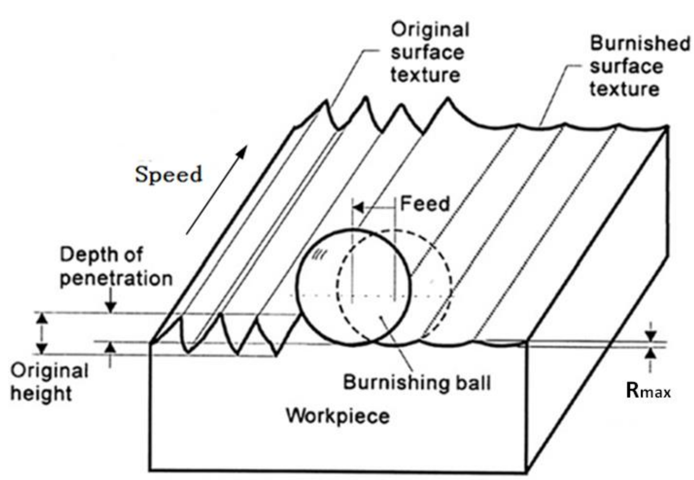

Figure 2-1 Sketch of ball burnishing process [13].

2.2.1 Studies on surface roughness

The effect of ball burnishing on surface roughness probably is the most commonly reported in literature reviews. The most parameters are concerned with pressure (or force), feed, and speed, in which pressure and feed usually have significant effects on surface roughness as opposed to the effect of speed which may be negligible [14, 56]. Rodríguez et al. [15] reported that commonly used mild steel AISI 1045 ball burnishing led to a smooth surface at Ra 0.3 μm similar to grinding and improved about 90% of surface roughness compared to the initial turned one. Prabhu et al. [58] investigated the effects of LPB and deep rolling on surface roughness of AISI 4140 steel (6 HRC) and discovered that among the four significant factors the improvements occurred with increases of force, ball diameter, and feed but decrease of initial roughness after LPB. In contrast, low level of force and initial roughness and high level of ball diameter and number of passes gave the best surface roughness in deep rolling process.

Pressure (force) plays a vital role in the burnishing process. From the beginning of the plastic deformation, an increase in pressure causes surface roughness to decrease until it reaches to a relatively lower value. It then tends to increase due to the overly high pressure which may result in over-burnished surface [10, 15, 20]. A study on several steels [13] showed that the optimal pressures of 15 MPa and 20 MPa on surface roughness were related to surface hardness ranges of less than 35 HRC and from 35 to 55 HRC, respectively, and also recommended higher pressure (more than 20 MPa) for harder materials (>50 HRC). An investigation on hard materials (>59 HRC) by Liviu et al. [14] revealed that higher pressure (38 MPa) resulted in better surface roughness. In addition, Li et al. [59] proposed a relation between surface roughness R_z and burnishing force that the decrease of surface roughness R_z was proportional to the square root of ball burnishing force, followed by an experimental analysis. Nevertheless, Neslusan et al. [60] showed that the influence of ball burnishing equipped with a 12 mm ball on surface roughness of hardened 100Cr6 bearing steel (62-64 HRC) was achieved with significant and relatively small improvements after hard turning with standard tools and with wiper tools, respectively, under additional parameters of a small force 40 N and 3-4 passes. Fu et al. [61] investigated ball burnishing mechanics on SE508 Nitinol alloy and observed that the depth of burnishing tracks increased from 0.2 to 4 μm under the increased pressure from 4 to 20 MPa with a good agreement between the prediction model and experiment measurements meanwhile the strain was from 0.01 to 0.2%.

Due to hydraulic pressure loss at the tip of the burnishing tool, applied force on the workpiece is smaller than the theoretical value converted from pressure, which was investigated on biomedical magnesium–calcium alloy by Salahshoor et al. [34] and found that the reduction increased with the increases of pressure, and the actual normal force was about 23% lower than the theoretical one. Furthermore, a linear relationship between pressure and actual normal force was found [4, 13] on a 6 mm ball burnishing tool by using a dynamometer.

Burnishing speed has a wide range introduced from 3 to 300 m/min [4] or between 10 and 250 m/min [13]. Luca et al. [4] recommended that usually values were lower than 150 m/min otherwise resulting in rougher surfaces which were also mentioned in the literature [28], and much lower speeds should be taken for rigid indentation tools. The value of 150 m/min also was introduced as the maximum established by the burnishing tool manufacturer [15]. Sagbas [27] and Tadic et al. [36] showed the speed had no significant influences on surface roughness of aluminum alloys, 7178 and EN AW-6082 (AlMgSi1) T651, respectively, moreover the same result was also found on mild steel AISI 1045 [15] which implied the feasible choice of maximum speed to save time.

Feed rate is also a very important factor for surface roughness because it is directly related to the surface profile which is highly dependent on tool contact geometry for soft materials (20~40 HRC) [5]. The relationship between feed and surface roughness (Figure 2-1) is given by the following equation (2-1) which represents an ideal situation ignoring the other effects such as flattening of ball, depth of penetration, changes in lubricating condition (causing upward flow), etc. [62].

$$R_{max} \cong \frac{f^2}{8R} \tag{2-1}$$

Where, R_{max} - height of intersection of two traces, f - feed, R- ball radius.

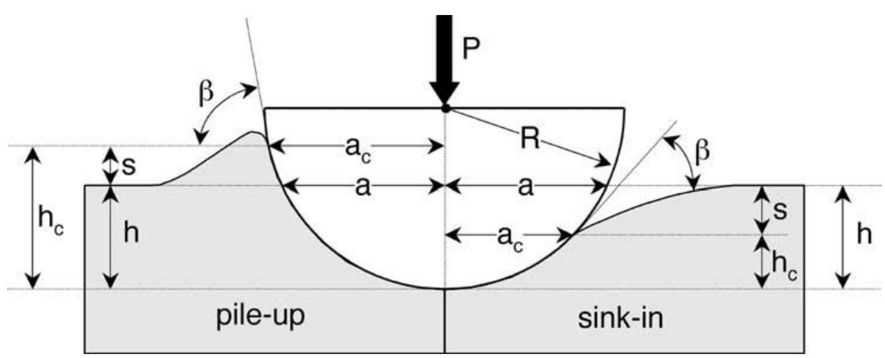

Figure 2-2 Geometry of spherical indentation with pile up and sink in [63].

Usually, the analysis of plastic deformation mechanics starts at indentation assumption based on Hertz theory (1896) for normal contact of elastic solids [63]. Taljat et al. [63] investigated contact geometry of spherical indentation with the phenomena of pile-up and sink-in shown in Figure 2-2, in which the FE simulation showed that these phenomena depended on the strain hardening exponent, n, in the empirical equation of Ludwik (1909) power law $\sigma = C\varepsilon^n$ (where σ is the stress, C is a constant stress, and ε is the strain) [52] and relative amount of elastic and plastic deformation.

Furthermore, Bouzid et al. [16] developed an analytical model for small feed values of ball burnishing on a cylindrical workpiece which showed that for small depth of penetration asperities were not eliminated but their heights were reduced shown in Figure 2-3, therefore, Eqs.2-1 was developed to Eqs.2-2 and 2-3.

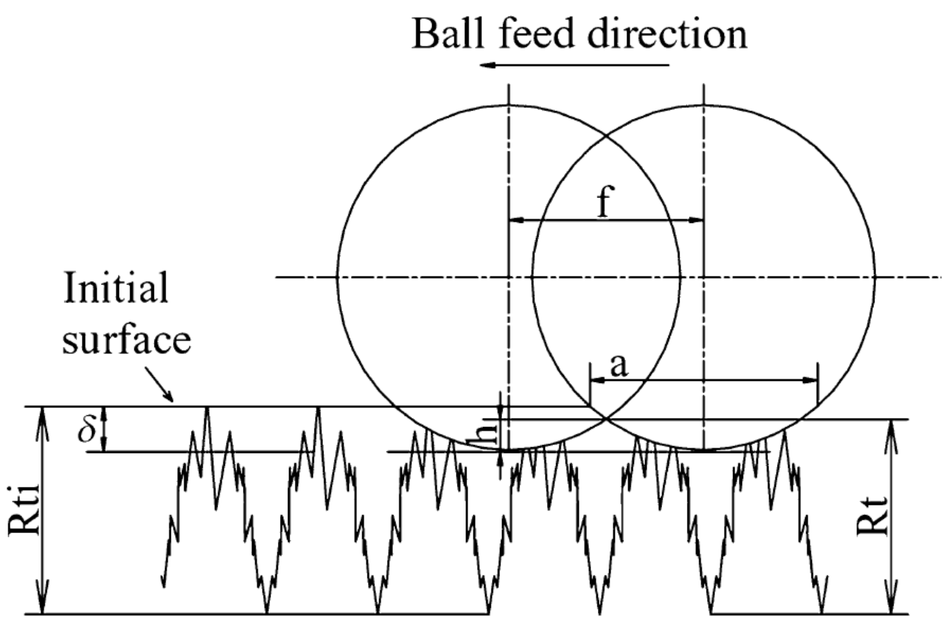

Figure 2-3 Sketch of ball burnishing on cylindrical workpiece (h≤ **δ**) [16].

$$R_t = R_{ti} - \delta + h \quad if\ \delta \leq R_{ti} \tag{2-2}$$

$$R_t = h \quad if\ \delta \geq R_{ti} \tag{2-3}$$

where, R_t- maximum height of surface roughness, R_{ti}- initial surface roughness, δ- normal displacement (h$< \delta < R_{ti}$), h=$\frac{f^2}{8R}$ (R is the ball radius, f is the feed).

Recently, Balland et al. [64] developed two numerical finite element models based on a mechanism of formation and flow of ridge to simulate the effect of ball burnishing processes. The first one on a smooth surface assumption in Figure 2-4 showed latter rolling action led to an increase at the bottom of the former groove and the bottom of the latter groove led to be slightly higher (distance x) thus regenerating the surface profile relative to roughness. Based on complex effects of processes on the second model for real surfaces, the author recommended accurate estimations might not be achieved.

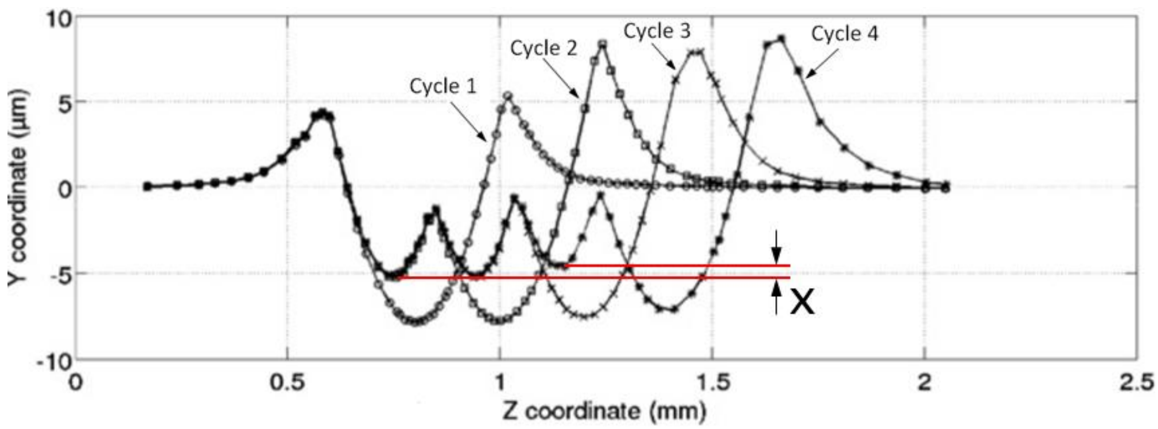

Figure 2-4 Surface profiles of ball burnishing modeling [64].

For number of passes, a previous research [25] revealed that a sufficiently good surface could be achieved by a single pass even though two or more passes might be better, which involved several steels with hardness from 31-52 HRC. Using a maximum force, one pass was suggested [4, 28]. For hardened steels, one pass was effective [4]. For soft materials, generally two or three passes resulted in the best surface finish [57, 58, 65, 66, 67] even though some cases preferred four passes on brass [24, 68], which was believed that a high number of passes could deteriorate surface finish due to over-hardening and consequently flaking of the surface layers [66].

For lubricant, it is more interesting to use machining coolant because of the burnishing process following machining. Machining coolant (emulsion of 3-5% oil in water) as pressure fluid was recommended for hydrostatic ball burnishing by the literature [10] in which an emulsion of 5% oil in water was applied in the experiment. Another study [15] employed an emulsion coolant of 3% oil in water. Nevertheless, many investigations focused on other lubricants such as SAE engine oil, kerosene, and diesel [56]. Hassan et al. [69] applied several lubricants by different viscosities from 8 to 413 mm^2/s (at 40°C), respectively, to mechanical ball burnishing process, and the results showed that there was no significant influence on surface roughness or on hardness during the change of viscosity of lubricants which also agreed with another research [58] on brake oil and gear oil applied to LPB and deep rolling processes. However, research [70] indicated a different result by using kerosene, SAE 30 oil, 5% and 10% graphite in SAE 30 oil that lighter oil resulted in better surface roughness.

Burnishing directions in NC milling machine was also studied by Salahshoor et al. [67] that smaller surface roughness was in parallel to burnishing track compared to that in perpendicular direction on Magnesium-Calcium alloy (MgCa0.8).

The empirical model is the most popular method to make functions determine the surface roughness [5, 71]. Tadic et al. [36] showed the study on surface roughness of aluminum alloy that the regression models were fitted successfully by the factors of burnishing force, feed, and number of passes with different initial roughness, in which the speed had no significant effect. However, their interactions may be taken into account. Sagbas [27] developed a regression model to predict surface roughness of 7178 aluminum alloy based on ball burnishing parameters of burnishing force, speed, feed, and number of passes by using response surface methodology (RSM) with central composite design (CCD), in which two main effects (force and number of passes) and five second-order interactions of the four parameters were significant on surface roughness, and there was only about 2.82% difference between experimental and predicted values.

2.2.2 Studies on surface hardness

The phenomenon of strain hardening appearing in most metals is a useful benefit for products which become stronger, harder, and consequently have larger influences on wear resistance and fatigue strength [36]. Due to the measurement of hardness by the indentation method as the most practical and useful method [53], investigations of ball burnishing focused on a type of penetration depth like Rockwell and another type of left impression such as Vickers and Knoop for hardness tests.

The studies on surface hardness involve ball burnishing parameters similar to those on surface roughness (section 2.2.1), e.g., Hassan et al. [65] showed normal force and the number of passes were the most effective factors on surface hardness among parameters such as speed, feed, etc. Usually, the increase of pressure or force increases the hardness [10, 13, 15, 65], in which the increase rate could slow down [65] or appear a proportional relationship [10]. By using Taguchi technique on brass [66], the contributions of influences of burnishing parameters on surface hardness were investigated that force (42.85%) and feed (29.3%) were the more significant parameters, followed by speed (13.95%) and number of passes (12.39%). The optimal hardness (the highest value) was obtained at highest force, medium feed, lowest speed, and highest number of passes.

Some investigations revealed that increasing pressure increases surface hardness (Rockwell) with the compatible results with microhardness, such as Vickers [10] and Knopp [13], which indicated that Rockwell hardness test could be enough accurate with its simplicity. However, as the burnishing force on magnesium-calcium alloy increased, a decrease of microhardness appeared at the surface with increases of microhardness in the subsurface [20]. Loh et al. [72] investigated microhardness profiles under two lubricants with the maximum hardness at about 0.2 mm depth below the surface and indicated that high force would reduce hardness due to excessive work hardening.

Hassan et al. [66] showed work hardening increased as the increases of number of passes (up to 5 passes) on commercial aluminum and brass with the further reduction of increase rates. Nevertheless, Rao et al. [24] indicated that the influence of number of passes (up to 5 passes) was proportional to surface hardness on brass (initial 59 HRB). Moreover, Hassan [68] showed that the increases of surface hardness of aluminum and brass were proportional to the force and number of passes, respectively. Loh et al. [28] recommended number of passes should be at one with maximum force or 2~3 at lower forces, otherwise a decrease in hardness attributed to surface deterioration by excessive work hardening. However, Gharbi et al. [17] showed that there was a little or no hardening effect of ball burnishing on micro hardness for ductile aluminum 1050A from 40 to 43 HV (50 g) by using a new tool which was designed for a large flat surface.

For mild steel AISI 1045, Seemikeri et al. [57] focused on four parameters that speed had the greatest influence on surface hardness followed by pressure, ball diameter and number of passes and high surface hardness was obtained at lower level of them by using LPB technique with a relatively low pressure. Prabhu et al. [58] compared the effects of

LPB and deep rolling on surface hardness of AISI 4140 steel (initial 6 HRC) that the improvements of 167% by LPB and 442% by deep rolling were achieved, in which surface hardness increased with increase of force and decreases of ball diameter and initial roughness in LPB whereas it increased with increases of force and ball diameter and decreases of initial roughness and number of passes. In the conclusion of this research, it is also recommended that higher surface hardness would be higher compressive residual stress consequently resulting in higher fatigue life. It should also be noted that the magnitude of surface hardness essentially depends on the amount of plastic deformation and compressive residual stresses during the burnishing process [1, 73].

Nemat et al. [74] also showed that the reduction of burnishing speed and feed rate led to increased hardness on steel and aluminum. However, a different result was achieved that speed and feed had no significant influence on surface hardness for the steel AISI 1045 [15].

For hardened steel, the maximum pressure and only one pass employed were effective and corresponding to the requirement of manufacturing productivity [4, 14]. A research [10] reported that increasing the burnishing pressure from 10 to 20 MPa on heat-treated steel improved surface hardness from 12.5% to 18.8% with initial hardness (32 HRC) and from 6.8% to 13.4% with initial hardness (41 HRC). Furthermore, GRZESIK et al [55] showed microhardness distributions by hard turning and hard burnishing within the depth of 100 μm on very hard steel (57 HRC) that even though high values of about 820 MPa microhardenss (HV0.05) at the surface and maximum value at about 80-100 μm depth generated by dry hard turning, subsequent ball burnishing caused harder maximum value (900 MPa) at the surface and harder subsurface layer up to about 70 μm depth followed by a gradual reduction. This phenomenon of near surface softening on very hard materials was also introduced by I. Altenberger [1].

2.2.3 Studies on residual stresses

Compressive residual stress plays a vital role directly related to fatigue life [13], together with tensile residual stress considered as macrostress which exits in multi-grain scale mainly responsible for the bulk properties of materials, compared to microstress which represents the second and third kinds of residual stress in the distance or range within one grain and between atoms, respectively, for microstructural properties shown in Figure 2-5 [75]. There are several methods for residual stress measurements, generally summarized into destructive and non-destructive techniques [75]. The former one includes hole drilling method, ring core technique, bending deflection method, the sectioning method. The later one includes the X-ray diffraction method, the neutron method, the ultrasonic method and the magnetic method. As one of the most commonly used methods, X-ray diffraction assisted with electro-polishing (EP) can measure residual stress profiles in the subsurface which is time-consuming and costly [75]. This also allows us to make more accurate evaluation for applications. Many studies focused on analysis of residual stress profiles with environmental approaches, such as EDM V-notch for FOD initiation, HCF test, salt medium for SCC corrosion [7, 8, 25, 37, 48, 50, 51]. For use of X-ray tube and {hkl} plane, the parameters may differ due to materials, e.g., a $\sin^2\psi$ technique and the X-ray diffraction of chromium Kα1 radiation from the (211) planes of steel for 17-4 PH martensitic stainless steel [7, 51] but different from other materials such as aluminum alloys [8, 37], titanium alloys [50], which also can be seen in a recommendation table given by Fitzpatrick et al. [76]. Furthermore, it is noted that a correction should be taken based on sample geometries after EP due to the relaxation of residual stresses [75].

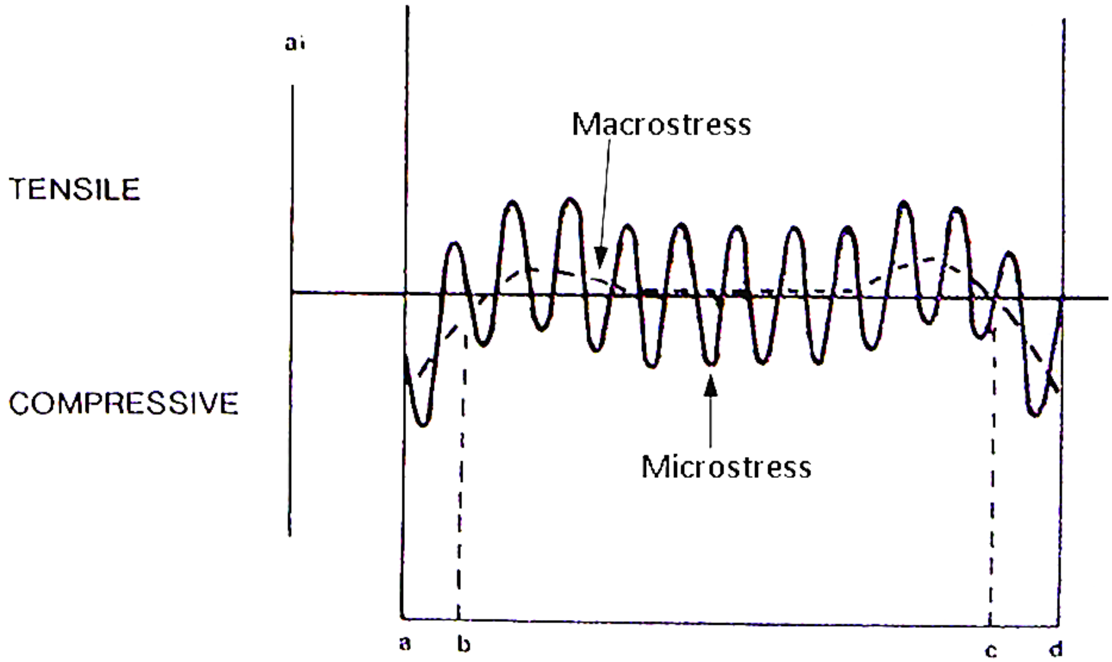

Figure 2-5 Residual stress profiles by Lu [75].

Since the elastic-plastic contact by ball burnishing is approximately the same in both circumferential and axial directions, the induced residual stress becomes stable [4]. In order to improve fatigue life and wear resistance, hardness and flow stress, good surface finish and compressive residual stresses are recommended as the keys [15]. Usually, round or both sides of samples for fatigue test are prior considered in order to avoid asymmetric residual stress distribution and bending influence [3]. Studies [2, 3] reported that ball burnishing produced a hook-shaped profile in deep compressive residual stress layer compared to SP, USP, and LSP on the heat treated Ti-2.5Cu and heat treated & double aging Ti-2.5Cu alloys with the highest value at the surface, in which higher circumferential residual stress was attained than axial one with the depths of maximum value about 150 μm and 200 μm, respectively. Moreover, the maximum and its depth were taken into account to be more important than the depth of compressive layer (up to zero-crossing depth) to improve HCF performance. However, Rodríguez et al. [15] indicated that axial residual stress was higher than tangential stress due to the burnishing directionality leading to higher plastic deformation in axial direction and these stresses mainly depended on burnishing pressure with similar results in both experiment and FE model in which higher pressure led to higher compressive residual stresses and a greater depth, followed by feed which had similar influence but low magnitude.

It is well known that compressive residual stress can inhibit crack nucleation and microcrack propagation [77]. Moreover, Prevéy et al. [48] revealed the effects of LPB on FOD and corrosion fatigue of 17-4 PH stainless steel that the significant improvement was attributed to high compressive residual stresses which delayed the initiation and early propagation of FOD cracks and maintained the stressed surface below the tensile threshold for corrosion fatigue. Wagner et al. [78] investigated fatigue performance of several alloys by the burnishing process which indicated that tensile residual stresses as the balance of compressive residual stresses appeared inhomogeneous distributions to cross-section with maximum value peaks resulting in similar crack nucleation sites (Figure 2-6) under a given burnishing pressure, observed in the HCF tests.

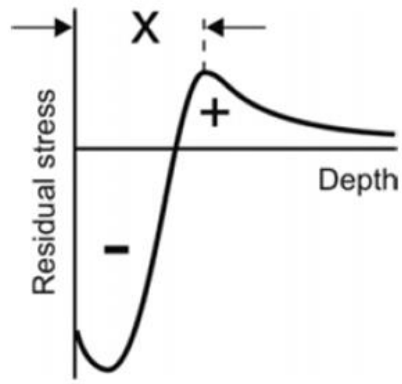

Figure 2-6 Residual stress profile after ball burnishing [78].

Furthermore, even though cold work can impede crack nucleation and may also accelerate microcrack propagation, compressive residual stresses retard the microcrack propagation which significantly contribute to the HCF while less effect on crack nucleation resistance [78]. On the other hand, Peters et al. [79] found that rare microcracks appeared around the damage sites of more ductile alloys like Ti-6Al-4V which gave an important potential to analyze the initial cracks of HCF for FOD. By using "feathering" technique which is used to prevent a high gradient from compressive to tensile stress fields and from tensile stress between compressive stress layers generated in operations, Luna et al. [80] invented a method to obtain a gradual compressive stress layer based on the depth of compressive residual stress layer controlled by process parameters. In addition, Luna et al. [81] showed the effort by using mechanical surface treatments including SP, LSP, pinch peening, and LPB to apply compressive residual stress patching to protect components from crack propagation which was a most interesting benefit for aerospace industry.

Using a milling machine, Gharbi et al. [17] investigated the effects of burnishing parameters on residual stress that increases of normal force improved the magnitude and depth of residual stress in feed direction but less effect in cross-feed direction. Furthermore, Salahshoor et al. [67] reported that residual stress along the burnished track is markedly smaller than that in perpendicular direction, and the optimal burnishing parameters in high compressive residual stress were obtained at low pressure, large feed, and fast speed with one pass. On Mg-Ca3.0 alloy, an investigation [22] showed that the increase of burnishing forces led to a decrease of residual stress magnitude at the surface and an increase of the maximum value depth whereas surface deterioration happened with excessive force (500N). In the application of titanium alloy for hip prosthesis [19], the magnitude of axial residual stress was about twice as that of circumferential one. On the other hand, this study indicated that low residual stress (compared to maximum stress in the subsurface) at the surface might reduce the beneficial influence of maximum residual stress on local fatigue during bending. Salahshoor et al. [21] investigated ball burnishing process mechanics in Mg-Ca0.8 alloy and built a FE model based on experimental analysis that the triaxial residual stresses were compressive below 200 μm depth with more compressive radial and circumferential residual stresses than axial one, and higher pressure increased their depth but had less effect on the magnitude. Moreover, Klocke et al. [32] built three FE models for plane, radii, and thin walled geometries, respectively with experimental analysis on residual stress induced by ball burnishing Ti-6Al-4V and IN718 aerospace metals, which showed very good correlations between predictions and experimental measurements.

The relaxation of compressive residual stress affected by temperature was investigated by Prevéy [82] and it was discovered that the stress relaxation mainly depended on the amount of cold work, thus less cold work resulted in higher thermal stability and, the most thermally stable compression was produced by the minimal cold work of LPB. In contrast, the increased yield strength by deep rolling with greater cold work may further improve fatigue life for low temperature applications.

The effect of low cycle fatigue (LCF) on residual stresses induce by deep rolling was also investigated. A study involving LCF under three conditions on AISI 304 and SAE 1045 steels was conducted by Nikitin et al. [83] that at high temperature deep rolling generated the most stable compressive residual stress, followed by deep rolling & annealing and conventional deep rolling (room temperature) thus longer fatigue life at elevated temperature would be obtained due to more stable microstructures. Gill et al. [84] found the relaxations of residual stresses induced by deep rolling on titanium alloys Ti-6Al-4V under LCF (room temperature), high temperature, and high temperature LCF with less than 50%, less than 40%, and ~70% decreases of maximum compressive residual stress, respectively, with no effect on depth of compressive layers. This research also showed the profile of the FWHM values of X-ray diffraction peaks empirically related to the level of plastic deformation or cold work that high level of cold work was imparted by deep rolling with the maximum plastic deformation at 100 μm depth.

Chapter 3

Experimental setup

3.1 Workpieces

The raw material was 17-4 PH stainless steel supplied as solution treated bright machining quality solid bars (Solution treated at 1038℃) in Ø1/2" x 6′ cut at 8 inch length. All the bars were heat-treated to the H1100 conditions (Figure 3-1): aged at a temperature of 593℃ (1100°F) for 4 hours, followed by air cooling.

Figure 3-1 Aging at 593℃ (1100°F) for 4 hours in the furnace, cooling in the air.

Finally, the average hardness was at 34.4 HRC (Correction was explained in section 4.2). The chemical composition shows as follows: Carbon ≤ 0.07%, Chromium 15~17.5%, Nickel 3~5%, Copper 3~5%, Manganese ≤ 1%, Silicon ≤ 1%.

The workpieces were turned by facing and center drilling and then were clamped on the CNC lathe (Romi Centur 35E with a GE Fanuc Series O-T CNC Control) shown in Figure 3-2 which includes three-jaw chuck, dead center, and tool turret equipped with a Valenite DNMG 432 LM VC919 carbide insert (nose radius of 0.031 in/0.8 mm). The turning parameters were controlled with a speed of 100 m/min (328 sfm), feed of 0.10 mm/rev (0.00394 in), and depth of cut of 0.008 inch. In addition, three extra turned samples were stored for the next steps.

Figure 3-2 View of burnishing process in the lathe.

3.2 Burnishing process

3.2.1 Set up of burnishing hydraulic system

The burnishing processes were carried out in the same lathe without unclamping the turned workpieces by using a ball burnishing tool mounted on the turret just next to the turning insert (Figure 3-2). The burnishing tool was set up at a distance X = 4 mm in Figure 3-3 (optional range of 1~5 mm shown in the ECOROLL operating instruction) without switching on the pump and against the workpiece edge under an applied pressure.

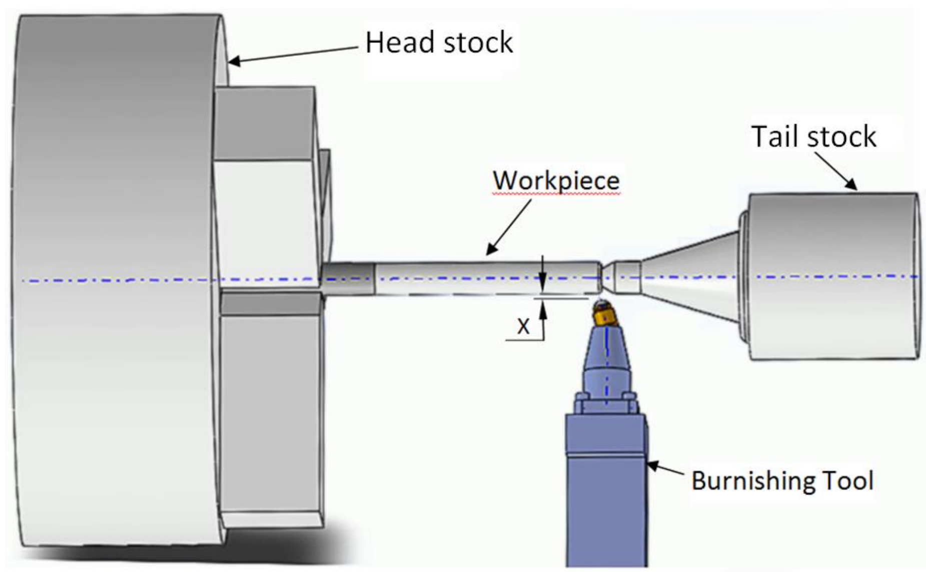

Figure 3-3 Sketch of ball burnishing process.

The ECOROLL HG6-9L15-SLK25 burnishing tool which is equipped with a 6 mm silicon nitride ceramic ball with a 15° angle in Figure 3-4 (a) is right for the CNC lathe with the short tool holder. The ECOROLL hydraulic system is shown in Figure 3-4 (b) in which a high pressure hydraulic pump HGP 4.3 can apply the maximum pressure up to 40 MPa. An emulsion-type coolant was mixed well with 5% oil content of TRIM® VHP® E814 soluble oil and 95% water by stirring devices. This emulsion is a low foaming, chlorine-free, long life, and versatile emulsion which can perform well in machining processes and especially excel in high-pressure environments (Master Chemical Co.).

(a) (b)

Figure 3-4 Burnishing devices: (a) burnishing tool, (b) Ecoroll hydraulic unit.

3.2.2 Design of experiment

In this study, a 3^3 factorial design was conducted by using Minitab software. The three quantitative factors selected were burnishing pressure, speed, and feed with three levels at numerical values, respectively (Table 3.1).

Table 3.1 Experimental levels of burnishing parameters.

Level	Pressure (MPa)	Speed (m/min)	Feed (mm/rev)
Low	12	40	0.06
Middle	18	70	0.10
High	25	100	0.15

3.3 Measurements of surface roughness

3.3.1 Set up

The values of mean surface roughness (Ra) before and after burnishing were measured by using FEDERAL® Pocket Surf® III portable surface roughness gage (cutoff =0.030 in/0.8 mm) which could be used without taking out workpieces after turning process. Cleaning work was necessary to avoid the effect of contamination by air and ethanol methods before measurements. The selection of traverse length was switched to 3 cutoffs (0.135 in/3.5 mm traverse length). For each workpiece, the average Ra was obtained by three measurements conducted along the longitudinal direction at different positions.

3.3.2 Fitting regression model

In this experiment, three variables were considered including pressure (P), speed (S), feed (F). In order to fit an empirical model [71], a functional relationship can be written as:

$$Ra = CP^{\alpha}S^{\beta}F^{\gamma} \tag{3-1}$$

Where, Ra –mean surface roughness;

C, α, β, γ – constant.

To solve the nonlinear equation (3-1), one of the most popular ways is to convert it into the following logarithmic form:

$$\ln(Ra) = lnC + \alpha lnP + \beta lnS + \gamma lnF \tag{3-2}$$

The Eq. above also can be rewritten as a linear mathematical equation:

$$\hat{y} = \beta_0 + \beta_1 x_1 + \beta_2 x_2 + \beta_3 x_3 \tag{3-3}$$

Where, $\hat{y}$ is the actual response (fitted value) of surface roughness on a logarithmic scale in which the random error (ϵ) exists in the logarithmic response (y) of measured values described as $\hat{y} = y - \epsilon$, and x_1, x_2,and x_3 are the logarithmic transformations of the burnishing pressure (P), speed (S), and feed (F), respectively, and β_0, β_1, β_2, and β_3 are the unknown parameters to be estimated.

After the first analysis by using experimental data, if the first-order model is not satisfactory, a second-order model is usually obtained by adding quadratic terms of the main factors as follows:

$$\hat{y} = \beta_0 + \beta_1 x_1 + \beta_2 x_2 + \beta_3 x_3 + \beta_{11} x_1^2 + \beta_{22} x_2^2 + \beta_{33} x_3^2 + \beta_{12} x_1 x_2 + \beta_{13} x_1 x_3 + \\ + \beta_{23} x_2 x_3 \tag{3-4}$$

In addition, the surface roughness (RaT) by turning can be a covariate in this model if necessary.

3.4 Measurement of impact strength

The turned and burnished specimens were cut in 3 inches. The V-notch of samples was cut in depth of 2 mm by using a 1-3/8 x 7/16 double angle cutter with 60 degree in HAAS VF-2 vertical NC machine center.

Charpy impact is one of the low velocity impact methods in energy absorption [85]. The tests were performed by using a Tinius Olsen pendulum type impact device shown in Figure 3-5 which was first verified without any specimen to make sure the reading was at zero point. Each sample was placed at the position with its notch opposite to the surface where the pendulum hit after release from its initial height by a lever.

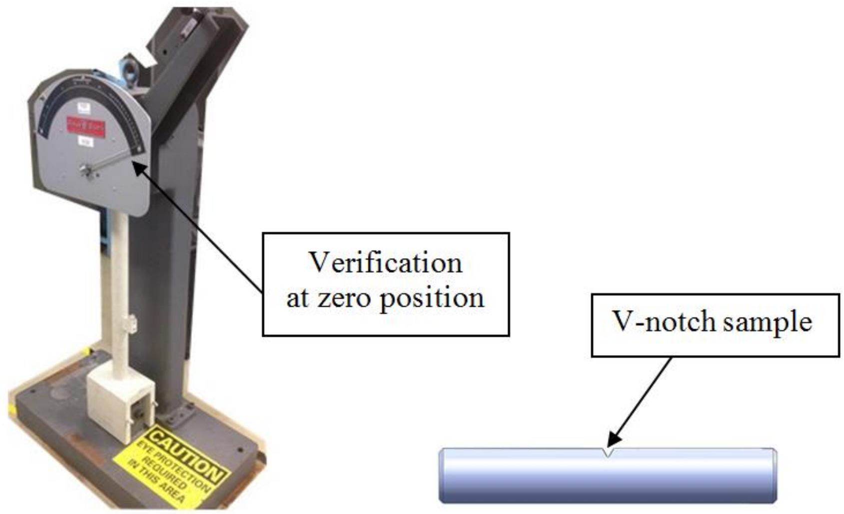

Figure 3-5 Charpy impact test device and V-notch sample.

3.5 Measurement of surface hardness

As one of the widely used methods, the Rockwell C hardness tests were conducted for the cylindrical specimens by using an Akashi ACCUPRO AR-10 hardness tester shown in Figure 3-6. The tester was switched on auto unload. The minor 10 kg load was first applied by rising up the sample stage, and then the major 150 kg loading and unloading were done by itself. All the tests were carried out at three circumferential points 120° apart for each part. According to ASTM E18 - 08b, Standard Test Methods for Rockwell Hardness of Metallic Materials1, the shape of the sample can affect its hardness reading. The correction of measurements should be carried out due to the cylindrical shape of the samples.

Figure 3-6 Rockwell hardness apparatus.

3.6 Measurement of residual stress

Residual stresses were measured using a PANalytical X'Pert PRO X-ray diffraction device in the instrumentation center of the University of Toledo by using X-ray diffraction and $sin^2\Psi$ method. In the X-ray diffraction spectrum, the compressive residual stresses result in peak displacement toward high angle position due to the decrease of interplanar spacing as opposite to low angle position of peak displacement due to the increase of interplanar spacing [75]. According to this, 2θ-$\sin^2\Psi$ method is the most popular to use in the measurement of residual stress as a sensitive and accurate technique [75]. In order to fit the chamber of the sample stage, a sample holder was machined to fix the specimens which were cut to 3/4 inch by using an abrasive cutter.

The X-ray was generated at the setting of 45 kV and 40 mA. Using a copper Kα source (λ=1.5418740 Å) from the (211) plane and $2\theta = 82.02^\circ$ in Figure 3-7 (a), the onedimensional scans were carried out with a point incident beam and a detector with a parallel plate collimator (0.27°) in 5 tilt angles (0° , 24.1° , 35.27° , 45° , and 54.74 °) for both positive and negative Ψ by using a sample stage of Open Eulerian Cradle. Due to only one positive Ψ movement of the sample stage, the negative Ψ was obtained by rotating a 180° φ angle (the horizontal plane) of the sample [76]. A sample fixed in the center of the holder was positioned at the true center of rotation of the Ψ and 2θ axes by using a dial gauge in Figure 3-7 (b).

According to Bragg's law, $2d\sin\theta = n\lambda\ (n\ is\ an\ integer)$, the change of lattice spacing due to the existence of residual stresses results in a peak shift after the rotation of a Ψ angle, and the shift magnitude is related to the magnitude of the residual stresses. The residual stresses were calculated by using factory defaults in PANalytical X'Pert Sress Plus software. For 17-4 PH stainless steel, the Yong's modulus (E) and Poisson ratio (ν) were chosen as 28.5 x10^6 psi (197 x10^3 MPa) and 0.272, respectively.

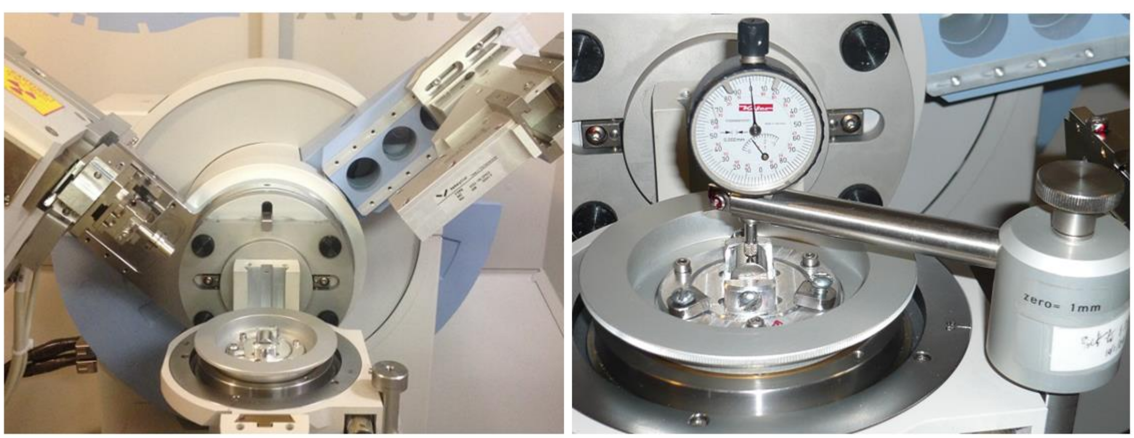

(a) (b)

Figure 3-7 Measurement of X-ray diffraction (a) Starting position (b) True center alignment.

In order to obtain residual stress profiles, electropolishing process was employed to minimize the effect of layer removal in several times to the depth of 1 mm, respectively. Due to the relaxation of residual stresses induced by layer removal, the three-dimensional residual stresses are corrected with equilibrium conditions of cylindrical symmetry by using equations as follows [75]:

$$\sigma_\theta(r_i) = \sigma_\theta^m(r_i) + \sigma_r(r_i); \tag{3-5}$$

$$\sigma_z(r_i) = \sigma_z^m(r_i) - 2\int_{r_i}^{r_0} \sigma_z^m(r)\frac{dr}{r}; \tag{3-6}$$

$$\sigma_r(r_i) = -\int_{r_i}^{r_0} \sigma_\theta^m(r)\frac{dr}{r}; \tag{3-7}$$

To solve the unknown functions $\sigma_\theta^m(r)$ and $\sigma_z^m(r)$, assuming linear relationships between the stresses and radius for each removal layer, the expressions can be described as $\sigma_\theta^m(r) = k_\theta r + \sigma_\theta$ and $\sigma_z^m(r) = k_z r + \sigma_z$, respectively, where $k_\theta, \sigma_\theta, k_z, \sigma_\theta$ are the constant coefficients. Thus, Eqs.3-6 and 3-7 can be rewritten as follows:

$$\sigma_r(r_i) = -\left\{\sigma_\theta^m(r_0) - \sigma_\theta^m(r_1) + \left(\sigma_\theta^m(r_0) - \frac{\sigma_\theta^m(r_0)-\sigma_\theta^m(r_1)}{r_0-r_1}r_0\right)\ln\left(\frac{r_0}{r_1}\right) + \sigma_\theta^m(r_1) - \sigma_\theta^m(r_2) + \left(\sigma_\theta^m(r_1) - \frac{\sigma_\theta^m(r_1)-\sigma_\theta^m(r_2)}{r_1-r_2}r_1\right)\ln\left(\frac{r_1}{r_2}\right) + \cdots + \sigma_\theta^m(r_{i-1}) - \sigma_\theta^m(r_i) + \left(\sigma_\theta^m(r_{i-1}) - \frac{\sigma_\theta^m(r_{i-1})-\sigma_\theta^m(r_i)}{r_{i-1}-r_i}r_0\right)\ln\left(\frac{r_{i-1}}{r_i}\right)\right\} \tag{3-8}$$

$$\sigma_z(r_i) = \sigma_z^m(r_i) - 2\left\{\sigma_z^m(r_0) - \sigma_z^m(r_1) + \left(\sigma_z^m(r_0) - \frac{\sigma_z^m(r_0)-\sigma_z^m(r_1)}{r_0-r_1}r_0\right)ln\left(\frac{r_0}{r_1}\right) + \sigma_z^m(r_1) - \sigma_z^m(r_2) + \left(\sigma_z^m(r_1) - \frac{\sigma_z^m(r_1)-\sigma_z^m(r_2)}{r_1-r_2}r_1\right)\ln\left(\frac{r_1}{r_2}\right) + \cdots + \sigma_z^m(r_{i-1}) - \sigma_z^m(r_i) + \left(\sigma_z^m(r_{i-1}) - \frac{\sigma_z^m(r_{i-1})-\sigma_z^m(r_i)}{r_{i-1}-r_i}r_{i-1}\right)\ln\left(\frac{r_{i-1}}{r_i}\right)\right\} \tag{3-9}$$

Where,

r_0 $-$ Initial radius;

$r_{1,}\ r_{2,}\ r_{i-1,}\ r_i$ $-$ Radii after 1st, 2nd, (i-1)st, ith layer removal;

$\sigma_\theta(r_i)$ $-$ True circumferential stress at radius r_i;

$\sigma_\theta^m(r_0),\ \sigma_\theta^m(r_1),\ \sigma_\theta^m(r_2),\ \sigma_\theta^m(r_{i-1}),\ \sigma_\theta^m(r_i)$ $-$ Measured circumferential stresses at radius r_0, r_1, r_2, r_{i-1}, r_i;

$\sigma_r(r_i)$ $-$ True radial stress at radius r_i;

$\sigma_z(r_i)$ $-$True axial stresses at radius r_i;

$\sigma_z^m(r_0),\ \sigma_z^m(r_1),\ \sigma_z^m(r_2),\ \sigma_z^m(r_{i-1}),\ \sigma_z^m(r_i)$ $-$ Measured axial stresses at radius r_0, r_1, r_2, r_{i-1}, r_i.

Moreover, the FWHM values in the measurements of X-ray peak broadening are carried out as the demonstration of the amount of plastic deformation or work hardening [1, 84].

Chapter 4

Results and discussions

This chapter presents the results of experimental study of the effects of ball burnishing on the surface integrity of 17-4 PH steel including surface roughness, hardness, and residual stresses. In addition, impact strength is also studied. Table 4.1 shows partial results of measurements in the experiments. The analysis is conducted by MINITAB 16 software.

4.1 Results and Analysis on Surface Roughness

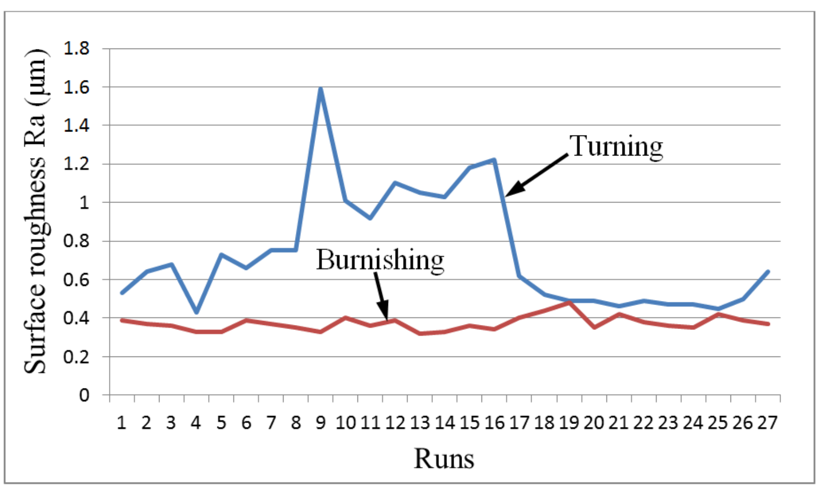

Figure 4-1 Surface roughness (Ra) obtained by turning and burnishing.

Figure 4-1 shows that the burnishing process reduces the surface roughness even though some values decrease slightly which is corresponding to the fact that the force applied by ball burnishing can smooth out the surface irregularities. Since the 17th run, the surface roughness modified by turning has been kept at low level due to the worn insert replaced by a new one.

Table 4.1 Results of turned surface roughness (RaT), burnished surface roughness (RaB), mean hardness, and impact strength after burnishing.

Sample	Pressure (MPa)	Speed (m/min)	Feed (mm/rev)	RaT (μm)	RaB (μm)	Hardness (HRC)	Impact strength (kgf.m).
B1	18	100	0.15	0.53	0.39	36.2	23.0
B2	12	100	0.15	0.64	0.37	35.8	26.3
B3	12	70	0.1	0.68	0.36	35.1	24.1
B4	12	40	0.1	0.43	0.33	35.9	22.1
B5	18	100	0.1	0.73	0.33	35.6	23.6
B6	18	40	0.15	0.66	0.39	35.4	24.2
B7	18	70	0.06	0.75	0.37	35.4	25.4
B8	18	40	0.06	0.75	0.35	35.8	21.9
B9	12	100	0.1	1.59	0.33	35.6	23.2
B10	12	70	0.15	1.01	0.40	35.3	24.05
B11	12	40	0.15	0.92	0.36	35.5	23.7
B12	25	70	0.06	1.10	0.39	36.7	22.3
B13	18	40	0.1	1.05	0.32	36.9	23.1
B14	12	40	0.06	1.03	0.33	35.5	24.0
B15	25	40	0.06	1.18	0.36	36.6	25.85
B16	18	70	0.1	1.22	0.34	36.2	23.25
B17	25	70	0.1	0.62	0.40	36.7	23.2
B18	25	100	0.15	0.52	0.44	35.8	24.2
B19	25	70	0.15	0.49	0.48	36.0	21.65
B20	12	70	0.06	0.49	0.35	35.6	24.7
B21	25	40	0.15	0.46	0.42	36.0	24.0
B22	25	100	0.1	0.49	0.38	36.2	25.6
B23	25	100	0.06	0.47	0.36	36.2	24.0
B24	18	100	0.06	0.47	0.35	36.4	22.5
B25	18	70	0.15	0.45	0.42	36.0	26.5
B26	25	40	0.1	0.50	0.39	36.2	22.45
B27	12	100	0.06	0.64	0.37	34.9	26.35

4.1.1 Effects of parameters on surface roughness

Table 4.2 shows in full ANOVA model the determination R^2 is about 98 percent as the rough explanation of the variability in the experiment. Considered with normal probability in Figure 4-2 (a) and residuals vs. fitted values in Figure 4-2 (b), this model is adequate. At α=0.05 level, the three main factors are significant. The turned roughness (RaT) concerned as a covariate is insignificant and when it's dropped, the 2-factor interaction of pressure and feed becomes significant (P value is 0.015 < 0.05).

Table 4.2 ANOVA for surface roughness by ball burnishing.

Analysis of Variance for RaB, using Adjusted SS for Tests

Source	DF	Seq SS	Adj SS	Adj MS	F	P	
RaT(covariate)	1	0.0066014	0.0000181	0.0000181	0.17	0.695	(Insignificant)
Pressure	2	0.0088464	0.0101439	0.0050720	46.84	0.000	
Speed	2	0.0043306	0.0041461	0.0020731	19.14	0.001	
Feed	2	0.0131360	0.0129025	0.0064512	59.57	0.000	
Pressure*Speed	4	0.0005684	0.0002237	0.0000559	0.52	0.727	(Insignificant)
Pressure*Feed	4	0.0013689	0.0013534	0.0003384	3.12	0.090	(0.015 without RaT)
Speed*Feed	4	0.0007243	0.0007243	0.0001811	1.67	0.259	(Insignificant)
Error	7	0.0007581	0.0007581	0.0001083			
Total	26	0.0363342					

S = 0.0104064   R-Sq = 97.91%   R-Sq(adj) = 92.25%

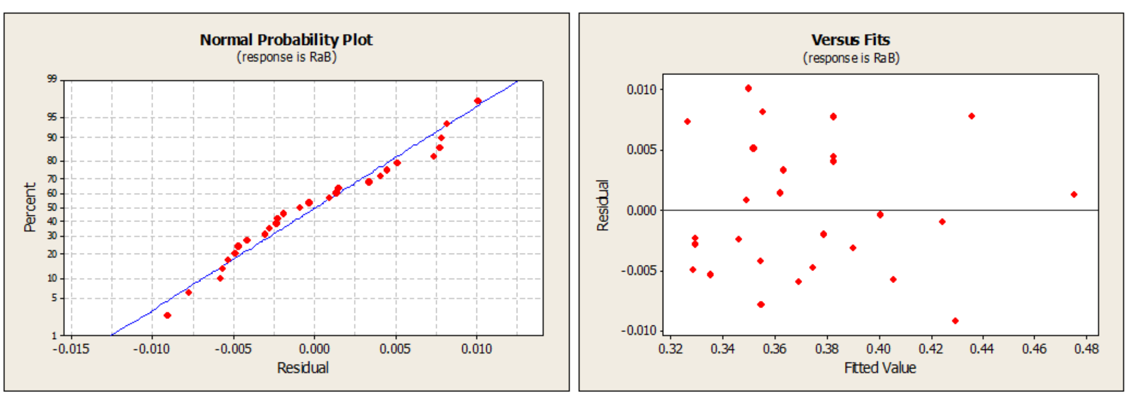

(a) (b)

Figure 4-2 (a) Normal probability plot of residuals, (b) plot of residuals versus fitted values.

The effect of burnishing pressure is shown in Figure 4-3(a) where the mean value of roughness increases as the increase of pressure. The critical effect of burnishing speed is shown in Figure 4-3(b). Surface roughness increases gradually to the highest value as speed increases from 40 m/min to 70 m/min and then decreases due to higher speed. In Figure 4-3(c), surface roughness slightly decreases as the increase of feed from 0.06 mm/rev close to 0.1 mm/rev and then increases quickly as feed increases continuously. Figure 4-3(d) shows some useful information regarding the effect of 2-factor interaction between pressure and feed; high pressure (25 MPa) consistently results in the roughest surface roughness in contrast to less variation of roughness at low level under the low pressure (12 MPa), and the lowest roughness values are achieved under pressure of 18 MPa, feed of 0.1 mm/rev.

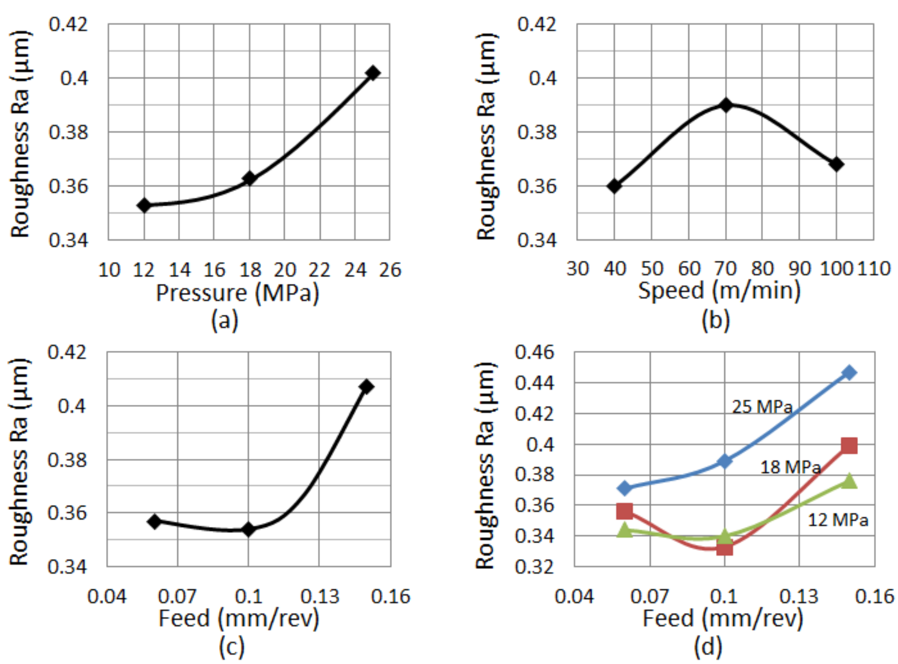

Figure 4-3 Plots of significant effects on burnishing roughness (Ra): (a) Roughness vs. Pressure, (b) Roughness vs. Speed, (c) Roughness vs. Feed, (d) 2-factor interaction between Pressure and Feed.

Apparently, higher pressure increases surface roughness. Increasing the applied pressure increases the amount of plastic deformation which not only reduces the heights of more asperities but also leads to the material moving upward [86] or pilling up in front of the ball [73] and larger waviness which may deteriorate the surface roughness [20] therefore surface roughness increases. The deteriorated trend on surface roughness can be indicated by the acceleration of increasing surface roughness from 18 MPa to 25 MPa in Figure 4-3 (a). The critical effect of speed can be attributed to the combined influence that surface irregularities increase due to chatter usually induced at higher speed; however, higher speed also results in less plastic deformation leading to better surface roughness [66, 73]. At feed from 0.06 to 0.1 mm/rev, lower feed leads to higher number of passes over the same site by the ball is more than that at high feed which can cause excessive work hardening resulting in poor finish based on much smaller feed than the track width and then a further increase in feed causes an increase of surface roughness which is the general consideration that surface profile is directly related to feed in ideal condition [28, 66]. The interaction influence is approximately corresponding to the previous explanations except for the optimal condition under 18 MPa and 0.1mm/rev. On the other hand, the high rates (in speed and feed) are possibly chosen to save process time in the manufacturing, and the determination of burnishing parameters also need to consider the results of next steps of this work.

4.1.2 Regression Analysis

Regression analysis is performed to establish an empirical model by using logarithmic transformation based on the experimental data shown in Table 4.3 that the three main factors and their four 2-factor interactions significantly affect surface roughness (RaB).

The determination (R^2 = 92.26%) of the second-order model reasonably explains the variability in the data [87]. The value of predicted R^2 is 84.11% which is not unreasonable with a consideration of the adjusted R^2 of 89.41%. As a comparison, Figure 4-4 shows the determinations of the first-order model are much lower than those in the second-order model, and the much higher value of PRESS (Prediction Error Sum of Squares) in the first-order model shown in Table 4.3 is also undesirable [87], whereas it indicates the effect of pressure which cannot be achieved in the second-order model.

Table 4.3 Regression analysis on surface roughness (RaB).

```
Regression Equation:
Ln(RaB)= -2.75336-1.45889Ln(P)+2.67084Ln(S)+1.59058Ln(F)+0.345112Ln(P)*Ln(P)
         +0.143497Ln(P)*Ln(F)-0.319186Ln(S)*Ln(S)+0.395212Ln(F)*Ln(F)

Analysis of Variance:
```

Source	DF	Seq SS	Adj SS	Adj MS	F	P	
Regression	7	0.225403	0.225403	0.0322004	32.3564	0.0000000	
Ln(P)	1	0.070097	0.006614	0.0066144	6.6465	0.0184263	(Pressure)
Ln(S)	1	0.004334	0.024554	0.0245542	24.6732	0.0000855	(Speed)
Ln(F)	1	0.067309	0.022693	0.0226935	22.8035	0.0001316	(Feed)
Ln(P)*Ln(P)	1	0.012632	0.012632	0.0126320	12.6932	0.0020772	
Ln(S)*Ln(S)	1	0.023962	0.023962	0.0239619	24.0780	0.0000979	
Ln(F)*Ln(F)	1	0.040027	0.040027	0.0400270	40.2209	0.0000044	
Ln(P)*Ln(F)	1	0.007042	0.007042	0.0070415	7.0756	0.0154651	
Error	19	0.018908	0.018908	0.0009952			
Total	26	0.244311					

Summary of the First-order Model: $Ra = 0.27065P^{0.169735}S^{0.0335967}F^{0.133181}$

```
S = 0.0667802     R-Sq = 58.02%        R-Sq(adj) = 52.54%
PRESS = 0.133817  R-Sq(pred) = 45.23%

Summary of the Second-order model:

S = 0.0315464      R-Sq = 92.26%        R-Sq(adj) = 89.41%
PRESS = 0.0388105  R-Sq(pred) = 84.11%
```

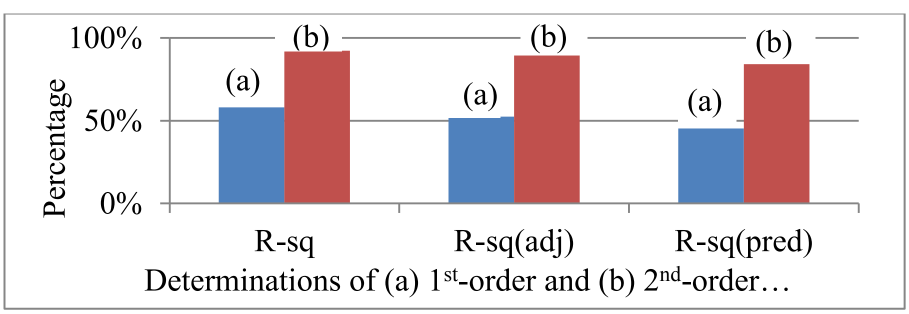

Figure 4-4 Differences of determinations between 1st and 2nd-order models.

As the result, a second-order empirical model is obtained as the form:

$$Ra = 0.06371P^{-1.45889}S^{2.67084}F^{1.59058}(e^{\ln P \ln P})^{0.345112}(e^{\ln P \ln F})^{0.143497}(e^{\ln S \ln S})^{-0.319186}(e^{\ln F \ln F})^{0.395212}$$

Where, e is the base of the natural logarithm. (4-1)

4.1.3 Validation

The purpose of the validation is to evaluate the accuracy of the prediction model with the experimental data. In this work, the prediction errors in Figure 4-5 are defined as follows:

$$\text{Prediction error} = \frac{\text{Pred. result} - \text{Exp. result}}{\text{Exp. result}} \times 100\% \tag{4-2}$$

The comparison of the prediction errors shows that the amplitude of errors in the second-order model is about ±5% which is acceptable, while the first-order model is about ±14%. These results are also corresponding to previous regression analysis.

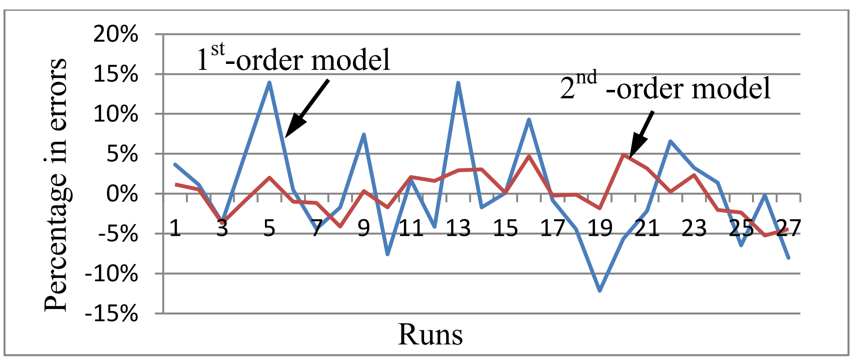

Figure 4-5 Prediction errors in the first-order and second-order models.

4.2 Results and analysis on surface hardness

Due to the measurement conducted on the cylindrical samples, all the hardness readings are corrected by using standard corrections on convex cylindrical surface (ASTM E18 -

08b). The result of the average values induced by ball burnishing is shown in Table 4.1. Based on this, Figure 4-6 shows the improvement of surface hardness in the range of 1.7% ~ 7.4%. Table 4.4 shows the result of ANOVA analysis where the pressure seems like the most efficient influence on surface hardness among these parameters which has a good agreement with previous work [15], whereas the determinations of the full model are relatively low, especially R-sq (adj), which may be attributed to the variations of surface hardness induced by the worn turning insert without being taken into account.

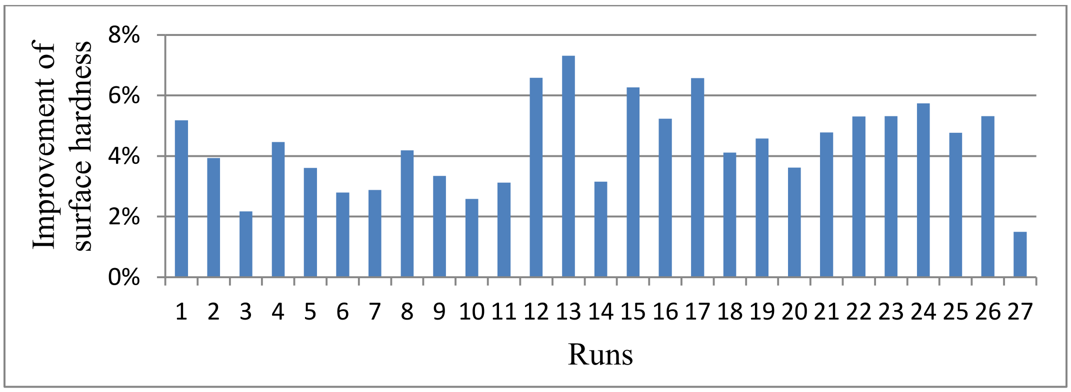

Figure 4-6 Improvement of surface hardness by ball burnishing.

Table 4.4 ANOVA for surface hardness variables.

Analysis of Variance for Hardness, using Adjusted SS for Tests

Source	DF	Seq SS	Adj SS	Adj MS	F	P	
Pressure	2	2.9956	2.9956	1.4978	6.60	0.020	**(Significant)**
Speed	2	0.0921	0.0921	0.0460	0.20	0.820	
Feed	2	0.3935	0.3935	0.1968	0.87	0.456	
Pressure*Speed	4	0.2832	0.2832	0.0708	0.31	0.862	
Pressure*Feed	4	0.5014	0.5014	0.1253	0.55	0.703	
Speed*Feed	4	0.5831	0.5831	0.1458	0.64	0.647	
Error	8	1.8150	1.8150	0.2269			
Total	26	6.6638					

S = 0.476309 R-Sq = 72.76% R-Sq(adj) = 11.48%

Figure 4-7 presents the effect of pressure on surface hardness where surface hardness increases at a percentage from 3.1% to 5.4% as the increase of the pressure. This improvement depends on two aspects, work hardening and compressive residual stresses induced [1]. Generally on the interpretation of work hardening, the increase of the amount of cold work leads to the increase of the material flow to valleys, compressions in more asperities, and consequently the increased density of dislocations [52] thus higher work hardening. Furthermore, at the high pressure (25 MPa) the increase rate of surface hardness tends to mitigate which may depend on the decreased generating rate of new dislocations at the high level and the influence of dislocation interactions increasing [52]. Nevertheless, the amount of work hardening may be relatively low due to low improvement of surface hardness and high compressive residual stresses existing in the surface layer shown in the section 4.4. The evaluation of work hardening will be reported in the section 4.4.5.

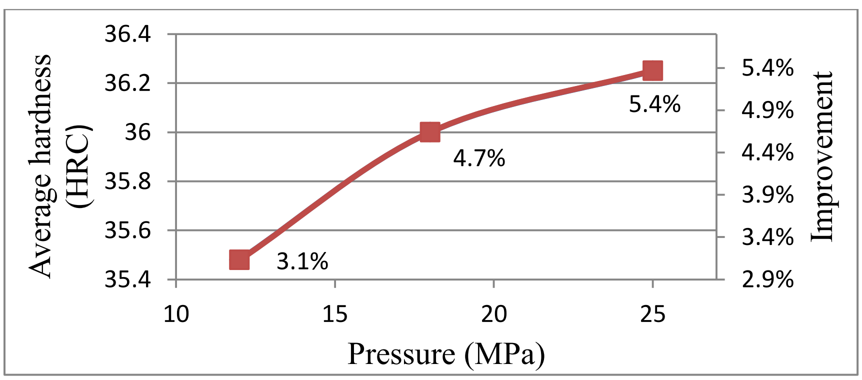

Figure 4-7 Effect of pressure on surface hardness and improvement.

4.3 Impact strength

The result of the impact strength measurements is shown in Table 4.1. The improvement is clearly seen in Figure 4-8 compared to the mean value (21.1 kgf.m) of the turned samples, and there are six values more than 20% which are more interesting for the next step of this work.

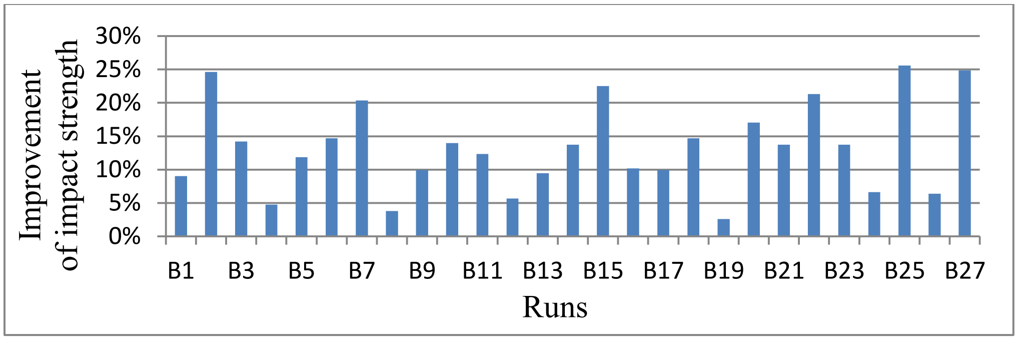

Figure 4-8 Improvement of impact strength by ball burnishing.

This should be explained carefully because generally work hardening reduces the impact toughness due to a decreased ductility; however, in this case the decrease may not be significant due to the superficial hardening which is a small part in the cross section of the sample and the possible low amount of work hardening mentioned in the section above and section 4.4.5. Moreover, deep compressive residual stresses with high magnitude (seen in section 4.4) can inhibit crack nucleation and microcrack propagation [77] as opposed to tensile residual stresses in turned samples shown in Figure 4-15. Therefore, the increase of impact strength may be mainly attributed to high compressive residual stresses induced. However, Figure 4-9 shows that the improvement of average impact strength at low pressure (12 MPa) is higher than those under pressures of 18 MPa and 25 MPa, even if higher compressive residual stresses are resulted from higher pressure. According to this, the impact strength or toughness defined as the ability to absorb energy comprises both strength and ductility and can be determined by the area surrounded by the stress-strain curve, fracture stress and strain [88], higher pressure leads to larger plastic deformation thus a smaller area left in the stress-strain curve plot denotes a lower toughness. More comments can be seen in the section 4.4.5.

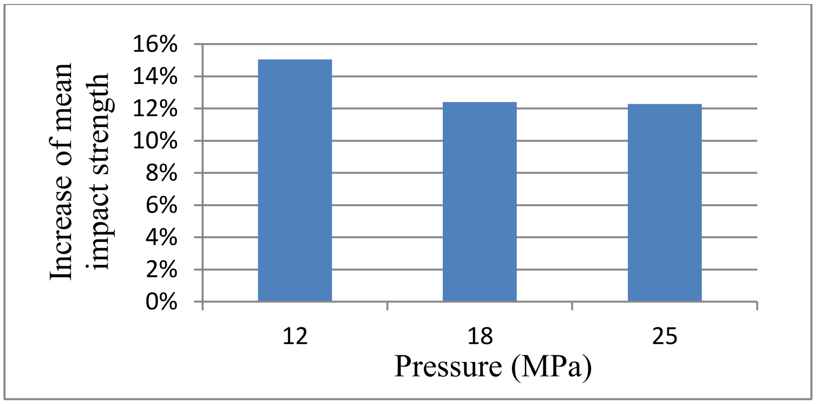

Figure 4-9 Increase of mean impact strength versus pressure.

4.4 Results and analysis of residual stress

4.4.1 Residual stresses at the surface

Table 4.5 and Table 4.6 show ANOVA analysis that only the pressure has a significant effect (α=0.05) on the circumferential and axial residual stress created at surface, respectively. Figure 4-10 indicates that the magnitude of both residual stresses at the surface increase as the pressure increases due to larger plastic deformation created.

Table 4.5 ANOVA for circumferential residual stress at the surface.

Analysis of Variance for $\sigma_{\theta\text{-}0}$, using Adjusted SS for Tests

Source	DF	Seq SS	Adj SS	Adj MS	F	P	
RaT	1	7898	2682	2682	0.31	0.596	
Pressure	2	635737	503664	251832	28.99	0.000	**(Significant)**
Speed	2	40232	47316	23658	2.72	0.133	
Feed	2	44935	52556	26278	3.02	0.113	
Pressure*Speed	4	101990	106863	26716	3.07	0.093	
Pressure*Feed	4	108723	105390	26347	3.03	0.095	
Speed*Feed	4	23240	23240	5810	0.67	0.634	
Error	7	60817	60817	8688			
Total	26	1023573					

S = 93.2100 R-Sq = 94.06% R-Sq(adj) = 77.93%

Table 4.6 ANOVA for axial residual stress at the surface.

Analysis of Variance for σ_{z-0}, using Adjusted SS for Tests

Source	DF	Seq SS	Adj SS	Adj MS	F	P	
RaT	1	2000	759	759	0.22	0.650	
Pressure	2	188516	148370	74185	21.98	0.001	**(Significant)**
Speed	2	6705	8789	4394	1.30	0.331	
Feed	2	8648	10987	5494	1.63	0.263	
Pressure*Speed	4	41423	43038	10759	3.19	0.086	
Pressure*Feed	4	54569	53833	13458	3.99	0.054	
Speed*Feed	4	11382	11382	2845	0.84	0.540	
Error	7	23629	23629	3376			
Total	26	336871					

S = 58.0991 R-Sq = 92.99% R-Sq(adj) = 73.95%

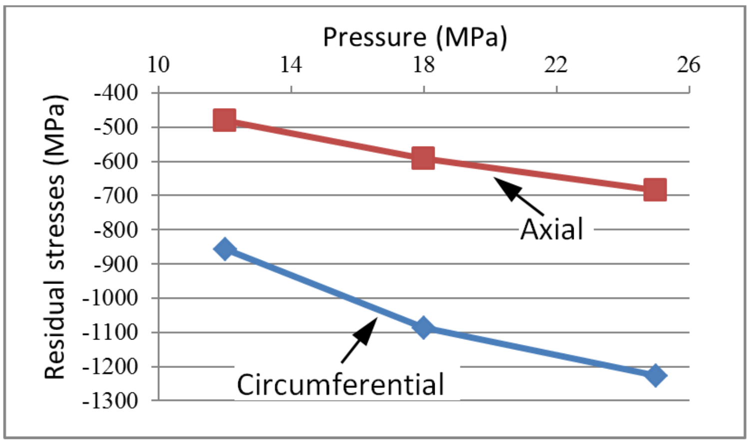

Figure 4-10 The effect of pressure on residual stresses at the surface.

4.4.2 Maximum residual stress and depths

Table 4.7 and Table 4.8 show that pressure is the only significant factor to affect maximum magnitude of circumferential residual stress and its depth as well as the result of axial residual stress presented in Table 4.9 and Table 4.10. The effects of pressure in Figure 4-11 shows that both maximum residual stresses increase as the pressure increases corresponding to the larger plastic deformation as the previous analysis, whereas, Figure 4-12 shows that low pressure (12 MPa) leads to a much deeper maximum than high pressure does which also depends on the contact geometry between the workpiece and the burnishing ball [1].

Table 4.7 ANOVA for maximum circumferential residual stress.

Analysis of Variance for $\sigma_{\theta\text{-}max}$, using Adjusted SS for Tests

Source	DF	Seq SS	Adj SS	Adj MS	F	P	
Pressure	2	216005	216005	108003	16.61	0.001	**(Significant)**
Speed	2	27718	27718	13859	2.13	0.181	
Feed	2	8584	8584	4292	0.66	0.543	
Pressure*Speed	4	27091	27091	6773	1.04	0.443	
Pressure*Feed	4	80124	80124	20031	3.08	0.082	
Speed*Feed	4	24371	24371	6093	0.94	0.489	
Error	8	52012	52012	6502			
Total	26	435906					

S = 80.6320   R-Sq = 88.07%   R-Sq(adj) = 61.22%

Table 4.8 ANOVA for depths of maximum circumferential residual stress.

Analysis of Variance for Depth-$\sigma_{\theta\text{-}max}$, using Adjusted SS for Tests

Source	DF	Seq SS	Adj SS	Adj MS	F	P	
Pressure	2	0.0237870	0.0237870	0.0118935	16.41	0.001	**(Significant)**
Speed	2	0.0049256	0.0049256	0.0024628	3.40	0.085	
Feed	2	0.0039423	0.0039423	0.0019711	2.72	0.126	
Pressure*Speed	4	0.0018839	0.0018839	0.0004710	0.65	0.643	
Pressure*Feed	4	0.0017273	0.0017273	0.0004318	0.60	0.676	
Speed*Feed	4	0.0075486	0.0075486	0.0018871	2.60	0.116	
Error	8	0.0057985	0.0057985	0.0007248			
Total	26	0.0496132					

S = 0.0269224   R-Sq = 88.31%   R-Sq(adj) = 62.02%

Table 4.9 ANOVA for maximum axial residual stress.

Analysis of Variance for $\sigma_{z\text{-}max}$, using Adjusted SS for Tests

Source	DF	Seq SS	Adj SS	Adj MS	F	P	
Pressure	2	32128	32128	16064	6.79	0.019	**(Significant)**
Speed	2	18817	18817	9408	3.98	0.063	
Feed	2	14296	14296	7148	3.02	0.105	
Pressure*Speed	4	2620	2620	655	0.28	0.885	
Pressure*Feed	4	1503	1503	376	0.16	0.953	
Speed*Feed	4	18923	18923	4731	2.00	0.187	
Error	8	18914	18914	2364			
Total	26	107200					

S = 48.6240   R-Sq = 82.36%   R-Sq(adj) = 42.66%

Table 4.10 ANOVA for depths of maximum axial residual stress.

Analysis of Variance for Depth-$\sigma_{z\text{-}max}$, using Adjusted SS for Tests

Source	DF	Seq SS	Adj SS	Adj MS	F	P	
Pressure	2	0.015140	0.015140	0.007570	5.34	0.034	**(Significant)**
Speed	2	0.007561	0.007561	0.003780	2.67	0.130	
Feed	2	0.003525	0.003525	0.001763	1.24	0.339	
Pressure*Speed	4	0.004425	0.004425	0.001106	0.78	0.568	
Pressure*Feed	4	0.007303	0.007303	0.001826	1.29	0.351	
Speed*Feed	4	0.004281	0.004281	0.001070	0.76	0.582	
Error	8	0.011337	0.011337	0.001417			
Total	26	0.053572					

S = 0.0376447   R-Sq = 78.84%   R-Sq(adj) = 31.22%

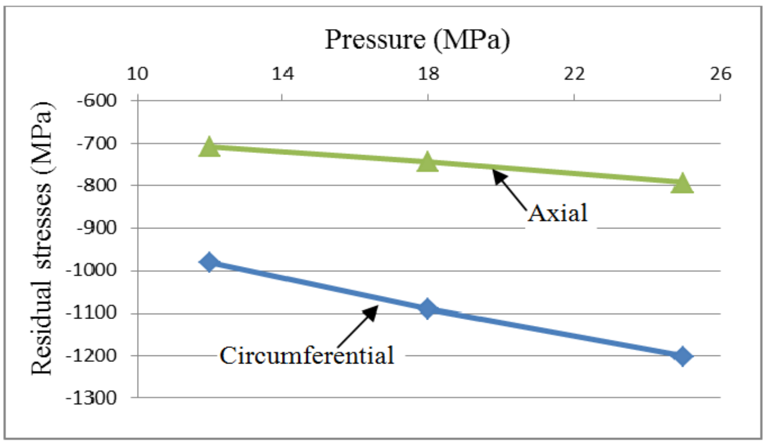

Figure 4-11 The effect of pressure on maximum residual stresses.

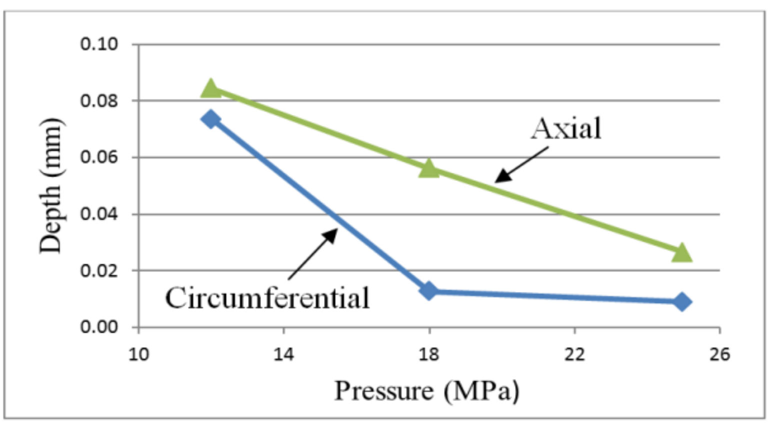

Figure 4-12 The effect of pressure on depths of maximum residual stresses.

4.4.3 Regression analysis

The regression analyses on residual stresses at the surface and their maximum magnitudes show that the determinations of the first-order models are at a relatively low rate of about 50 % ~ 67 % without fitting second-order models since no significant effects from any second-order factors. The empirical models of circumferential ($RS_{\theta-0}$) and axial (RS_{z-0}) residual stresses at the surface and for maximum values of circumferential ($RS_{\theta-max}$) and axial (RS_{z-max}) residual stresses are presented as follows:

$$RS_{\theta-0} = -250.4\, P^{0.496473} \qquad (4\text{-}3)$$

$$RS_{z-0} = -143.6\, P^{0.484656} \qquad (4\text{-}4)$$

$$RS_{\theta-max} = -496.7\, P^{0.27233} \qquad (4\text{-}5)$$

$$RS_{z-max} = -537.9\, P^{0.102332} \qquad (4\text{-}6)$$

In these models, the positive exponents (< 1) indicate that increasing pressure will increase the magnitudes of residual stresses at reduced rates. Equations 4-3 and 4-4 show that residual stresses at the surface are approximately proportional to the pressure to the power of 1/2. Nevertheless, the validations of these models in Figure 4-13 show the inaccurate results with the amplitudes of their errors at about 36.6%, 36.3%, 17.5%, and 18.7% and their average errors at the values of 10.6%, 10.7%, 6.7%, and 6.4%, respectively. Therefore, the models on residual stresses would be recommended for the qualitative analysis.

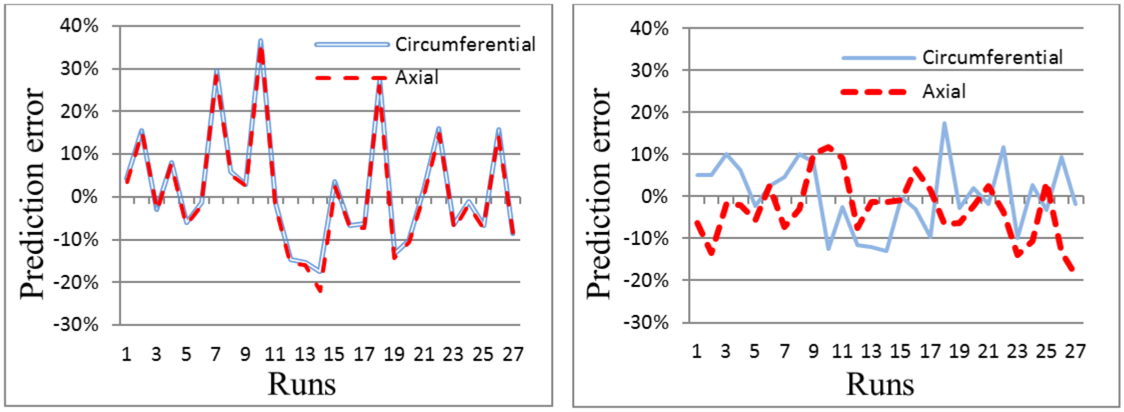

(a) (b)

Figure 4-13 Prediction errors of residual stresses (a) at the surface (b) for maximum magnitude.

4.4.4 Residual stress profiles

With high improvement of impact strength, six samples are measured to determine the residual stress profiles. Figure 4-14 ~ 4-16 show the results of the triaxial residual stress distributions for ball burnishing. Clearly, both the depths of circumferential and axial residual stresses are more than 1 mm, and the radial residual stress from zero at the surface is always tensile in the subsurface and proportional to the depth.

Under pressure of 12 MPa, Figure 4-14 (a) shows that the circumferential residual stress increases from a value of -743.8 MPa at the surface to a maximum value of -929.1 MPa at a depth of 0.11 mm, and the axial residual stress starts at a value of -415.8 MPa at the surface and increases to a depth of 0.1 mm with a maximum value of -802.3 MPa, followed by gradual decreases. Similar plots are achieved at a different feed of 0.06 mm/rev in Figure 4-14 (b). The circumferential residual stress increases from a value of -941.3 MPa at the surface to the maximum of -994.6 MPa at the depth of 0.1 mm and the magnitude of axial residual stress increases from -525.6 MPa at the surface to a maximum value of -853.7 MPa at the depth of 0.1 mm.

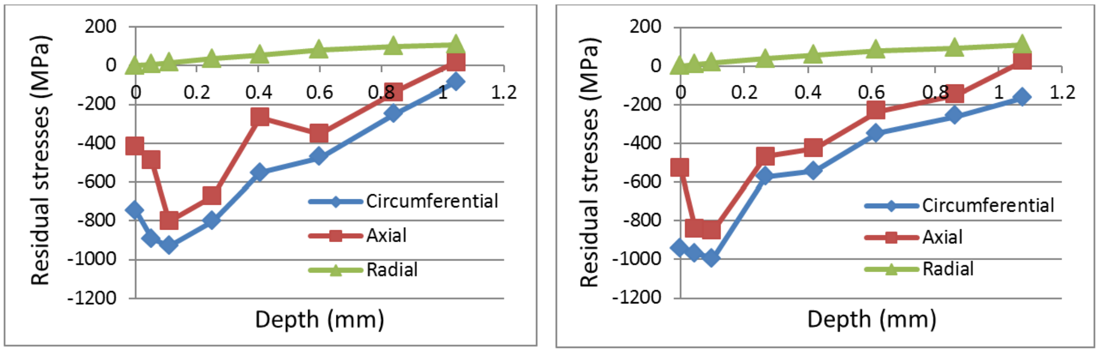

(a) (b)

Figure 4-14 Distributions of triaxial residual stresses at 12 MPa, 100 m/min (a) 0.15 mm/rev (b) 0.06 mm/rev.

Under pressure of 18 MPa and speed 70 m/min, Figure 4-15 (a) shows triaxial residual stress profiles at the feed of 0.06 mm/rev. The circumferential residual stress has a value of -812.3 MPa at the surface but sharply increases to the maximum value of -1042.2 MPa at a depth of 0.013 mm, followed by a gradual decrease. The axial residual stress starts with a value of -454.1 MPa at the surface and reaches to a maximum value at the depth of 0.065 mm. In Figure 4-15 (b) at a high feed of 0.15 mm/rev, the maximum circumferential residual stress occurs at the surface with a value of -1127.7 MPa, and there is a small peak found at the depth of 0.11 mm with the second maximum value of -810 MPa. For axial residual stress, the magnitude varies from a value of -629.5 MPa at the surface to a value of -417.7 MPa at a depth of 0.044 mm and then to the maximum value of -698.5 MPa at the depth of 0.11 mm.

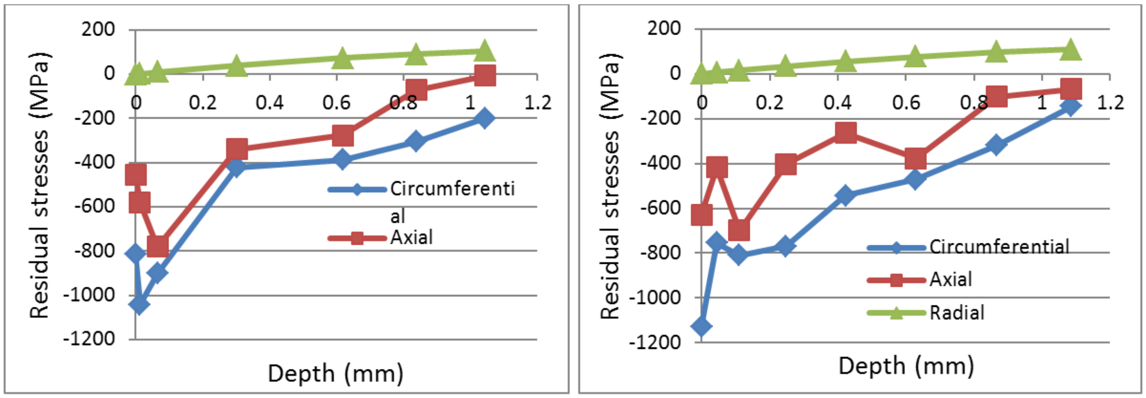

(a) (b)

Figure 4-15 Distributions of triaxial residual stresses at 18 MPa, 70 m/min, and (a) 0.06 mm/rev (b) 0.15 mm/rev.

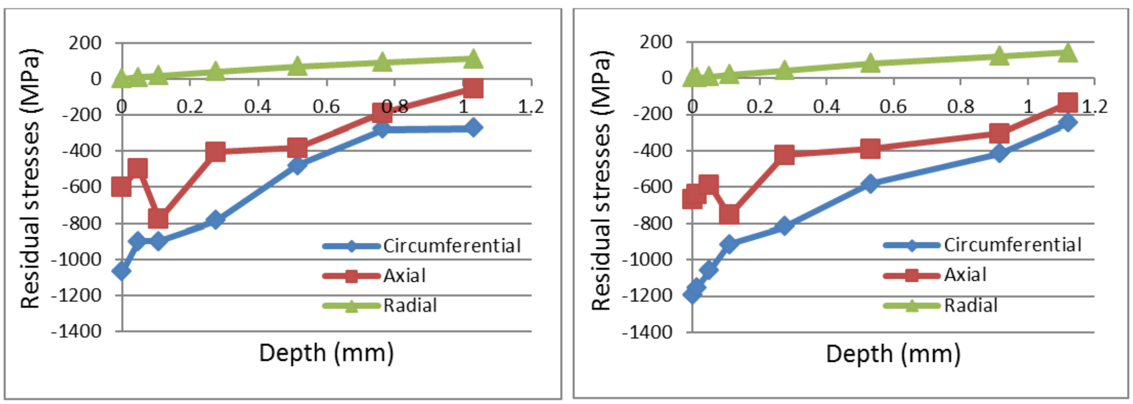

(a) (b)

Figure 4-16 Distributions of triaxial residual stresses at (a) 25 MPa, 100 m/min, and 0.1 mm/rev and (b) 25 MPa, 40 m/min, and 0.06 mm/rev.

Under the parameters of 25 MPa, 100m/min, Figure 4-16 (a) and (b) show the results at a feed of 0.1 mm/rev and 0.06 mm/rev, respectively. For circumferential residual stresses, the maximum values occur at both surfaces with a value of -1067.9 MPa in (a) and a value of -1194 MPa in (b), followed by the gradually decrease values as the increases of the depths. In Figure 4-16 (a), the axial residual stress varies from a value of -596.3 MPa at the surface to -496.5 at a depth of 0.048 mm and then to the maximum value of -777.7 MPa at the depth of 0.11 mm, followed by a decrease as the depth increases. In Figure 4-

16 (b), the maximum axial residual stress occurs at the surface. As the depth increases, the magnitude first decreases to a value of -588.5 MPa at 0.05 mm and then increases to -623 MPa at a depth of 0.11 mm, followed by a gradual decrease.

As a comparison, Figure 4-17 shows the profiles of residual stresses resulted by pre-machining, turning, which generates tensile stresses in the near surface (depth ≤18 μm). The magnitude of radial residual stress is very small. For circumferential residual stress, the tensile stress was generated from a value of 143.2 MPa at the surface to a maximum value of 299.2 MPa at a depth of about 8 μm. Beyond 18 μm, the residual stress becomes compressive and has a maximum value of -360.9 MPa at about 30 μm and then gradually decreases to a slightly compressive value -77.2 MPa at a depth of 50 μm. Similar profile for axial residual stress is achieved, but the magnitude is smaller than that of circumferential residual stress.

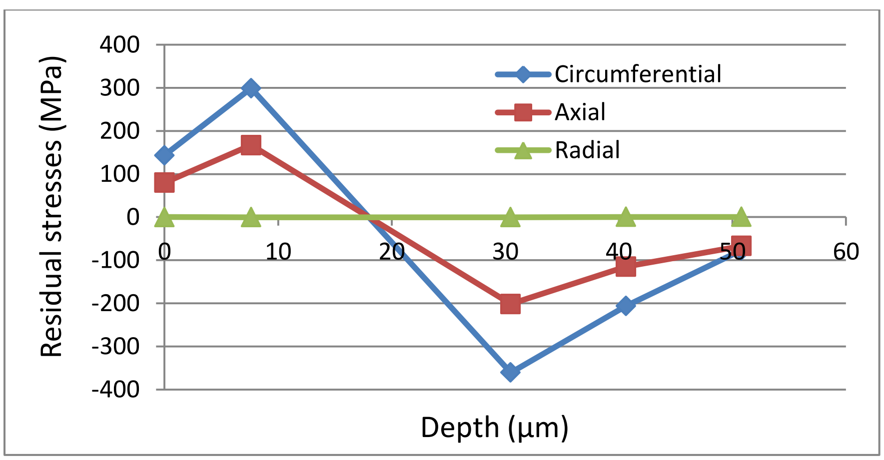

Figure 4-17 Distributions of triaxial residual stresses by turning.

Compared to the results in Figure 4-17 generated by turning, the burnishing process transforms tensile residual stresses into compressive residual stresses and induces much higher magnitude and deeper compressive layers over 1 mm, which noticeably impede microcrack propagation [79] considered as a contribution to the improvement of impact strength. In addition, the compressive residual stresses in a horizontal plane are anisotropic which leads to a circumferential residual stress more compressive than axial residual stress.

It is obvious that under the pressure of 12 MPa the distributions of both circumferential and axial residual stresses appear desirable hook-shaped profiles where the maximum residual stresses occur in the subsurface, which are very common for the burnishing process [89] and considered beneficial for service life [90].

In contrast, as the pressure increases, the magnitude of the maximum circumferential residual stress tends to increase with a decrease of its depth. In addition, even though the profiles shown in Figure 4-13 (a) look hook-shaped, the depths of maximum value is shallow, especially the circumferential one. It can be assumed that one of the reasons is that impact strength did not increase consistently with the high level of residual stresses. Another reason that may be considered is microcrack nucleation possibly occurred in transition region due to a high balancing tensile stress increasing the probability of microcrack occurrence [3].

4.4.5 Work hardening

Figure 4-18 shows that the average FWHM values under burnishing pressure appear three stages as increases of the depths: quick decreases from the surface to the depth of about 10 μm, followed by a variation to the depth of about 0.11 mm, and gradual decreases with the further increases of depths. As a comparison, the plot of the FWHM values by turning shows a quick decrease to the depth of about 30 μm, followed by a gentle decline.

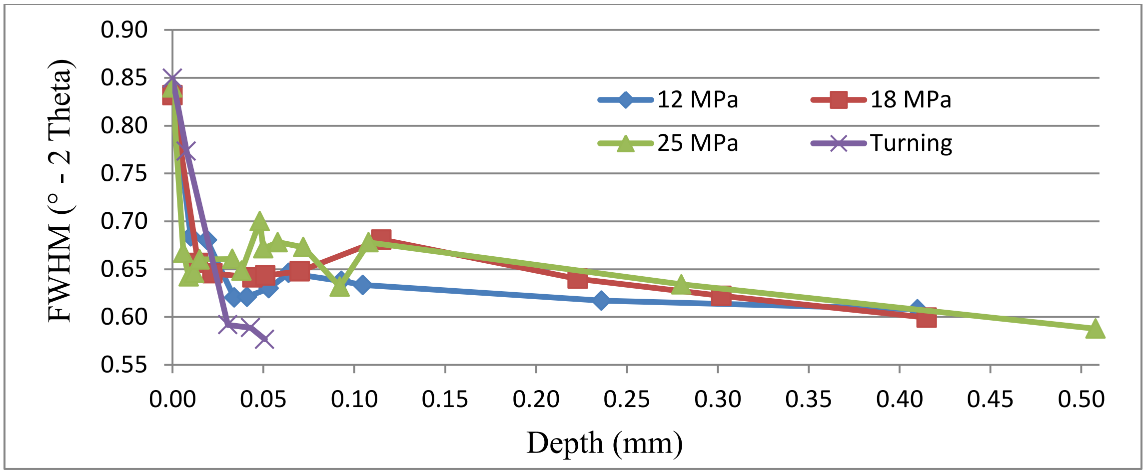

Figure 4-18 Effects of burnishing pressure on the FWHM values compared with the result by turning.

Since the FWHM values are related to the work hardening states [1, 84], it is obvious that even though turning also results in a thin layer of work hardening, more work hardening in the subsurface layer is induced by burnishing and consequently increases surface hardness. This evidence indicates that burnishing improves work hardening, and the amount of work hardening does not show an overly high level, which also supports the analysis of the improvement of impact strength. Moreover, from surface to the depth of about 20 μm a minor softening occurs during the burnishing process compared to the turning, and higher pressure leads to a slightly further softening. For the bulk FWHM values, higher pressure leads to higher FWHM values thus induces a higher amount of work hardening and consequently decreases impact strength. Nevertheless, Figure 4-9 shows the average impact strengths under 18 MPa and 25 MPa are almost same, which can be interpreted that the negative effect of the slightly higher FWHM values under 25 MPa is compensated by higher compressive residual stresses. On the other hand, no significant increases of the FWHM values under high pressure are indicated because low generated rate of new dislocations is corresponding to the analysis of a slow improvement rate of surface hardness at 25 MPa. Furthermore, the lower FWHM values under 12 MPa show the evidence of higher impact strength and lower surface hardness.

Chapter 5

Conclusions and future work

5.1 Conclusions

This study investigates the effects of ball burnishing on surface integrity of aerospace material 17-4 PH steel. The results indicated the significance of ball burnishing application for the aerospace blade material. The following conclusions can be drawn:

- The burnishing process leads to a smoother surface on which significant effects of process parameters that include pressure, feed, and speed are obtained, whereas the influence of turned surface roughness is negligible.
- A second-order empirical model on surface roughness (Ra) that was established has compatibility with the experimental results.
- Both surface hardness and impact strength are improved while higher pressure leads to a higher surface hardness, and lower pressure tends to have a higher impact strength, considering the pressure is the most important factor.

- High compressive residual stresses with a greater depth of layer are achieved, and higher pressure tends to have a higher magnitude of maximum compressive residual stresses, but a shallower depth. The results showed that hook-shaped residual stress profiles are achieved under low pressure.
- The X-ray peak broadening values (FWHM) indicate the evidence of the work hardening state which supports the analyses of surface hardness and impact strength.

5.2 Future work

- For deep understanding, the study of microstructure is recommended.
- High cycle fatigue (HCF) tests can help the analysis assisted with notch simulation of crack initiation induced by foreign object damage (FOD).
- For more accurate results of residual stresses, the highest possible 2-theta angle would be set up by using chromium radiation in X-ray diffraction.
- Flat sample may be chosen to cover the application of flat geometry.

References

[1] I. Altenberger, Deep rolling – The past, the present and the future. ICSP9: SHOT PEENING 2006.

[2] E. Maawad, H.-G. Brokmeier, L. Wagner, Y. Sano, Ch. Genzel Investigation on the surface and near-surface characteristics of Ti–2.5Cu after various mechanical surface treatments. Surface & Coatings Technology 205 (2011) 3644–3650.

[3] E. K. S. Maawad Residual Stress Analysis and Fatigue Behavior of Mechanically Surface Treated Titanium Alloys. HZG Report 2013-1.

[4] Liviu Luca, Investigations into the Use of Ball-Burnishing of Hardened Steel Components as a Finishing Process, PhD dissertation 2002, University of Toledo.

[5] Sorin Neagu-Ventzel A Theoretical and Experimental Study of Single Roll Burnishing Process as Applied to Yokes. PhD dissertation August, 2001, University of Toledo.

[6] Liviu Luca, Sorin Neagu-Ventzel, Ioan Marinescu Burnishing of hardened steel components – An alternative method of finishing. Proceedings of the annual meeting-American society for precision engineering; 110-114, 2002.

[7] Paul S. Prevéy, N. Jayaraman, Ravi Ravindranath Low plasticity burnishing (LPB) treatment to mitigate FOD and corrosion fatigue damage in 17-4 PH stainless steel. Proceedings of the Tri-Service Corrosion Conference Las Vegas, NV, November 17-21, 2003.

[8] Jeremy Scheel, Paul Prevéy and Douglas Hornbach Prevention of Corrosion Related Failure of Aircraft Aluminum Using an Engineered Residual Stress Field. DoD Corrosion Conference 2011.

[9] B. Karpuschewski, H.-J. Pieper, F. Welzel, K. Risse Alternative strategies in finishing cylinder running surfaces. CIRP Annals - Manufacturing Technology 61 (2012) 559–562.

[10] L. N. López de Lacalle, A. Lamikiz, J. A. Sánchez and J. L. Arana The effect of ball burnishing on heat-treated steel and Inconel 718 milled surfaces. Int J Adv Manuf Technol (2007) 32: 958–968.

[11] Fang-Jung Shiou, Chuing-Hsiung Chuang Precision surface finish of the mold steel PDS5 using an innovative ball burnishing tool embedded with a load cell. Precision Engineering 34 (2010) 76-84.

[12] Yinggang Tian, Yung C. Shin Laser-assisted burnishing of metals. International Journal of Machine Tools & Manufacture 47 (2007) 14-22.

[13] L.N. López de Lacalle, A. Lamikiz, J. Muñoa, J.A. Sánchez Quality improvement of ball-end milled sculptured surfaces by ball burnishing. International Journal of Machine Tools & Manufacture 45 (2005) 1659–1668.

[14] Liviu Luca, Sorin Neagu-Ventzel, Ioan Marinescu Effects of working parameters on surface finish in ball-burnishing of hardened steels. Precision Engineering 29 (2005) 253-256 2007.

[15] A. Rodríguez, L.N. López de Lacalle, A. Celaya, A. Lamikiz, J. Albizuri Surface improvement of shafts by the deep ball-burnishing technique. Surface & Coatings Technology 206 (2012) 2817–2824.

[16] W. Bouzid, O. Tsoumarev, K. Saï An investigation of surface roughness of burnished AISI 1042 steel. Int J Adv Manuf Technol (2004) 24: 120–125.

[17] Fathi Gharbi & Salem Sghaier & Hedi Hamdi &Tarek Benameur Ductility improvement of aluminum 1050A rolled sheet by a newly designed ball burnishing tool device. Int J Adv Manuf Technol (2012) 60:87–99.

[18] N.S.M. El-Tayeb ∗, K.O. Low, P.V. Brevern Influence of roller burnishing contact width and burnishing orientation on surface quality and tribological behaviour of Aluminium 6061. Journal of Materials Processing Technology 186 (2007) 272-278.

[19] Alexander Schuh, Christian Zeller, Ulrich Holzwarth, Werner Kachler, Gerhard Wilcke, Gu¨ nther Zeiler, Bernd Eigenmann, Jean Bigoney Deep Rolling of Titanium Rods for Application in Modular Total Hip Arthroplasty. 2006 Wiley Periodicals, Inc. J Biomed Mater Res Part B: Appl Biomater 81B: 330–335, 2007.

[20] M. Salahshoor & Y. B. Guo Surface integrity of magnesium-calcium implants processed by synergistic dry cutting-finish burnishing. Procedia Engineering 19 (2011) 288 – 293.

[21] M. Salahshoor & Y. B. Guo Process mechanics in ball burnishing biomedical magnesium–calcium alloy. Int J Adv Manuf Technol DOI 10.1007/s00170-012-4024-4 @Springer-Verlag London Limited 2012.

[22] B. Denkena (2), A. Lucas Biocompatible Magnesium Alloys as Absorbable Implant Materials –Adjusted Surface and Subsurface Properties by Machining Processes. Annals of the CIRP Vol. 56/1/2007.

[23] Shu Yang, Oscar W. Dillon, Jr., David A. Puleo, Ibrahim S. Jawahir Effect of cryogenic burnishing on surface integrity modifications of Co-Cr-Mo biomedical alloy. J Biomed Mater Res Part B 2012:00B:000–000.

[24] J.N. Malleswara Rao, A. Chenna Kesava Reddy and P. V. Rama Rao Experimental investigation of the influence of burnishing tool passes on surface roughness and hardness of brass specimens Indian Journal of Science and Technology Vol. 4 No. 9 (Sep 2011).

[25] Jeremy E. Scheel and Douglas J. Hornbach The effect of surface enhancement on improving the fatigue and sour service performance of downhole tubular components. Lambda Technologies Proceedings of the ASME 2012 International Mechanical Engineering Congress & Exposition IMECE2012 November 9-15.

[26] Ecoroll Tools & Solutions for Metal Surface Improvement.
www.ecoroll.com/downloads/kat/ecoroll_katalog_de_web.pdf

[27] Aysun Sagbas Analysis and optimization of surface roughness in the ball burnishing process using response surface methodology and desirabilty function. Advances in Engineering Software 42 (2011) 992–998.

[28] N. H. Loh and S. C. Tam Effects of ball burnishing parameters on surface finish- A literatrue survey and discussion. Precision Engineering October 1988 VOL 10 NO 4.

[29] Pande, S.S., Patel, S.M. Investigations on vibratory burnishing process. Int. J. Mach. Tool. Des. Res. 24, 195–206. 1984.

[30] D. S. Georgiev Increasing of the Oil Retentiveness Capability of Working Surfaces of Ship's Shafts Sliding Bearings, by Using of Vibratory Burnishing as Finishing Processing Manufacturing Engineering/ Vyrobne Inzinierstvo, 2009.

[31] A. Moshkovich, V. Perfilyev, K. Yutujyan, L. Rapoport Friction and wear of solid lubricant films deposited by different types of burnshing. Wear 263 (2007) 1324-1327

[32] F. Klocke, V. Bäcker, H. Wegner, A. Timmer Innovative FE-analysis of the roller burnishing process for different geometries. X International Conference on Computational Plasticity ® CIMNE, Barcelona, 2009.

[33] C. Richard Liu Roller-burnished parts. Design for manufacturability handbook Chapter 4.17 page 4.199-4.206. 1998.

[34] Michael Prevey, Paul S. Prevey, III Burnishing Tool and Method for Burnishing Published No.: US 2012/0104390 Al.

[35] A.A. Ibrahim, S.M. Abd Rabbo, M.H. El-Axir, A.A. Ebied Center rest balls burnishing parameters adaptation of steel components using fuzzy logic. Journal of materials processing technology 2 0 9 (2 0 0 9) 2428–243.

[36] Branko Tadic & Petar M. Todorovic & Ognjan Luzanin & Dragomir Miljanic & Branislav M. Jeremic & Bojan Bogdanovic & Djordje Vukelic Using specially designed high-stiffness burnishing tool to achieve high-quality surface finish. Int J Adv Manuf Technol DOI 10.1007/s00170-012-4508-2 Springer-Verlag London Limited 2012.

[37] Paul S. Prevéy, John Cammett "Low cost corrosion damage mitigation and improved fatigue performance of low plasticity burnished 7075-T6. Journal of Materials Engineering Performance, vol. 10(5) Materials Park, OH; ASM International, Oct., 2001, pp. 548-555".

[38] Marinescu, I., Dontu, G., Neagu-Ventzel, S. Dimitrov, B. Study of the Tip Burnishing Process Applied on Hardened Steels, Intertech 2000 Conference, Vancouver.

[39] Mieczyslaw Korzynskia, Janusz Lubas, Slawomir Swirad, Kazimiera Dudek Surface layer characteristics due to slide diamond burnishing with a cylindrical-ended tool. Journal of Materials Processing Technology 211 (2011) 84–94.

[40] J T Maximov, G V Duncheva, I M Amudjev and T V Kuzmanov Modelling the power parameters of the spherical motion burnishing. Proceedings of the Institution of Mechanical Engineers, Part C: Journal of Mechanical Engineering Science 2012 226:521 originally published online 6 October 2011.

[41] P. S. Pa Continuous finishing processes using a combination of burnishing and electrochemical finishing on bore surfaces. Int J Adv Manuf Technol (2010) 49:147-154.

[42] Mieczyslaw Korzynski Relief making on bearing sleeve surface by eccentric burnishing. Journal of materials processing technology 2 0 9 (2 0 0 9) 131–138.

[43] Tim J Carter Common Failures in Gas Turbine Engines. Engineering Failure Analysis 12 (2005) 237–247.

[44] V. Infante, J.M. Silva, M. de Freitas, L. Reis Failures analysis of compressor blades of aeroengines due to service. Engineering Failure Analysis 16 (2009) 1118–1125.

[45] www.birdstrike.org, Bird Strike Committee USA. July 31, 2013.

[46] E. Silveira, G. Atxaga, A.M. Irisarri Failure analysis of a set of compressor blades. Engineering Failure Analysis 15 (2008) 666–674.

[47] Boyce, Meherwan P. Gas Turbine Engineering Handbook. Published by Gulf Professional Boston, MA, 3rd edition, 2006.

[48] Paul S. Prevey, Dr. Nayarananan Jayaraman, Ravi Ravindranath Mitigation of FOD and Corrosion Fatigue Damage in 17-4 PH Stainless Steel Compressor Blades with Surface Treatment. 9th National Turbine Engine High Cycle Fatigue Conference 2004.

[49] J.D. Bressana,∗, D.P. Darosa, A. Sokolowskib, R.A. Mesquitac, C.A. Barbosa Influence of hardness on the wear resistance of 17-4 PH stainless steel evaluated by the pin-on-disc testing. journal of materials processing technology 2 0 5 (2 0 0 8) 353–359.

[50] Paul S. Prevéy, N. Jayaraman, Ravi A. Ravindranath Hcf performance and fod tolerance improvement inti-6al-4v vanes with LPB treatment. Proceedings 42nd AIAA Aerospace Sciences Meeting Reno, NV, January 5-8, 2004, Vol. 9, No. 1-4, 2004 Meeting Papers. Lambda Technologies.

[51] Paul S. Prevey, Dr. Nayarananan Jayaraman, Ravi Ravindranath Fatigue life extension of steam turbine alloys using low plasticity burnishing (LPB). Proceedings of ASME Turbo Expo 2010: Power for Land, Sea and Air GT2010-22995.

[52] J. Chakrabarty Theory of Plasticity. Third edition published by Elsevier Butterworth-Heinemann 2006 Pages 1-10.

[53] Milton C. Shaw Metal cutting principles. Published by Oxford University Press Inc., New York. Reprinted 1997.

[54] Michael Ashby, Hugh Shercliff, David Cebon Materials: Engineering, Science, Processing and Design. Published by Elsevier Ltd. First edition 2007 Page 132.

[55] Wit GRZESIK, Krzysztof ZAK, Mariusz PRAZMOWSKI Surface integrity of hard turned parts modified by ball burnishing. Journal of Machine Engineering, Vol. 12, No. 1, 2012.

[56] Deepak Mahajan, Ravindra Tajane A Review on Ball Burnishing Process. International Journal of Scientific and Research Publications, Volume 3, Issue 4, April 2013.

[57] C.Y. Seemikeri, P.K. Brahmankar, S.B. Mahagaonkar Investigations on surface integrity of AISI 1045 using LPB tool. Tribology International 41 (2008) 724–734.

[58] P. R. Prabhu, S. M. Kulkarni, S. S. Sharma Influence of deep cold rolling and low plasticity burnishing on surface hardness and surface roughness of AISI 4140 steel. World Academy of Science, Engineering and Technology 48 2010.

[59] Feng Lei Li, Wei Xia, Zhao Yao Zhou, Jing Zhao, Zheng Qiang Tang Analytical prediction and experimental verification of surface roughness during the burnishing process. International Journal of Machine Tools & Manufacture 62 (2012) 67–75.

[60] Miroslav NESLUSAN, Wit GRZESIK, Krzysztof ZAK Analysis of surface roughness on bearing steel parts after cutting, superfinishing and burnishing operations. Journal of Machine Engineering, Vol. 12, No. 1, 2012.

[61] C.H. Fu, Y.B. Guo, J. McKinney, and X.T. Wei Process Mechanics of Low Plasticity Burnishing of Nitinol Alloy. JMEPEG (2012) 21:2607–2617.

[62] N. H. Loh, S. C. Tam and S. Miyazawa Investigations on the surface roughness produced by ball burnishing. Int. J. Mach. Tools Manufact. Vol. 31, No. 1. Pp. 75-81. 1991.

[63] B. Taljat and G.M. Pharr Development of Pile-up During Spherical Indentation of Elastic-Plastic Solid, Int. J. Solids Struct., 2004, 41, p3891–3904.

[64] Pascale Balland, Laurent Tabourot, Fabien Degre, Vincent Moreau Mechanics of the burnishing process. Precision Engineering 37 (2013) 129–134.

[65] Adel Mahmood Hassan, Aiman Sharef A1-Bsharat Improvements in some properties of non-ferrous metals by the application of the ball-burnishing process. Journal of Materials Processing Technology 59 (1996) 250-256.

[66] T. A. El-Taweel & M. H. El-Axir Analysis and optimization of the ball burnishing process through the Taguchi technique. Int J Adv Manuf Technol (2009) 41:301–310.

[67] M. Salahshoor, Y.B. Guo Surface integrity of biodegradable Magnesium–Calcium orthopedic implant by burnishing. Journal of the Mechanical Behavior of Biomedial Materials 4 (2011) 1888–1904.

[68] Adel Mahmood Hassan The effects of ball- and roller-burnishing on the surface roughness and hardness of some non-ferrous metals. Journal of Materials Processing Technology 72 (1997) 385–391.

[69] Adel Mahmood Hassan, Ayman Mohammad Maqableh The effects of initial burnishing parameters on non-ferrous components. Journal of Materials Processing Technology 102 (2000) 115-121.

[70] U M Shirsat & B B Ahuja Parametric analysis of combined turning and ball burnishing process. Indian Journal of Engineering & Materials Sciences Vol. 11, October 2004, pp. 391-396.

[71] Cuthbert Daniel, Fred S. Wood FITTING EQUATIONS TO DATA: computer Analysis of Multifactor Data. Second Edition 1980 by John Wiley & Sons, Inc.

[72] N. H. Loh, S. C. Tam and S. Miyazawa Surface hardening by ball burnishing. TRIBOLOGY INTERNATIONAL 0301-679X/90/060413©-5 1990.

[73] N.S.M. El-Tayeb, K.O.Low,P.V.Brevern. On the surface and tribological characteristics of burnished cylindrical Al-6061. Tribology International 42 (2009) 320-326.

[74] Nemat M, Lyons AC An investigation of the surface topography of ball burnished mild steel and aluminium. Int J Adv Manuf Technol 16:469–473 (2000).

[75] Jian Lu Handbook of Measurement of Residual Stresses. Society for Experimental Mechanic, Inc. 1996 Pages 1-4, 77-132.

[76] M.E. Fitzpatrick, A.T. Fry, P. Holdway, F.A. Kandil, J. Shackleton and L. Suominen Determination of Residual Stresses by X-ray Diffraction – Issue 2. Measurement Good Practice Guide No. 52 © Crown copyright 2005, ISSN 1744-3911.

[77] M.M. El-Khabeery, M.H. El-Axir Experimental techniques for studying the effects of milling roller-burnishing parameters on surface integrity. International Journal of Machine Tools & Manufacture 41 (2001) 1705–1719.

[78] Lothar Wagner, Tomasz Ludian, and Manfred Wollmann Ball-Burnishing and Roller-Burnishing to Improve Fatigue Performance of Structural Alloys. Engineering Against Fracture: Proceedings of the 1st Conference, Springer Science+Business Media B.V. 2009.

[79] J. O. Peters, O. Roder, B. L. Boyce, A. W. Thompson, and R. O. Ritchie "Role of foreign object damage on thresholds for high-cycle fatigue in Ti-6Al-4V. July 1999 Report No. UCB/R/99/A1166 Submitted to Metallurgical and Materials Transactions A".

[80] Alberto Luna, Joshua Leigh Miller Component of variable thickness having residual compressive stresses therein, and method therefor. Patent, Date of publication: 02.01.2008 Bulletin 2008/01.

[81] Alberto Luna, Michael Jay Brunck Method for Determining Initial Burnishing Parameters. Patent No.: US8,079,120 B2 Dec. 20, 2011.

[82] Paul S. Prevéy "The effect of cold work on the thermal stability of residual compression in surface enhanced IN718. Proceedings: 20th ASM Materials Solutions Conference & Exposition St. Louis, Missouri, October 10-12, 2000".

[83] Nikitin l., Besel M. Correlation between residual stress and plastic strain amplitude during low cycle fatigue of mechanically surface treated austenitic stainless steel AISI 304 and ferritic–pearlitic steel SAE 1045. Mater Sci Eng A 491:297–303 (2008).

[84] C M Gill, N Fox and P J Withers Shakedown of deep cold rolling residual stresses in titanium alloys. J. Phys. D: Appl. Phys. 41 (2008) 174005 (5pp).

[85] W.J. CANTWELL and J. MORTON The impact resistance of composite materials---a review. 0010-4361/91/050347-16 © 1991 Butterworth-Heinemann Ltd COMPOSITES. VOLUME 22. NUMBER 5. SEPTEMBER 1991 347.

[86] Afef Bougharriou &Wassila Bouzid Saï & Kacem Saï Prediction of surface characteristics obtained by burnishing. Int J Adv Manuf Technol (2010) 51:205-215.

[87] Douglas C. Montgomery Design and Analysis of Experiments. 7th Edition, 2009 Pages 75-97.

[88] B. K. Agrawal Introduction to Engineering Materials. Tata McGraw-Hill Education, 1988 – Materials, Pages 15-16.

[89] Patrick J. Golden, Alisha Hutson, Vasan Sundaram, James H. Arps Effect of surface treatments on fretting fatigue of Ti–6Al–4V. International Journal of Fatigue 29 (2007) 1302–1310.

[90] Kamil Kolarik, Zdenek Pala, Libor Beranek, Nikolaj Ganev Application of X-ray diffraction in development of new type of moulds for production of refraction of refractory and highly abrasive objects. Modern Machinery (MM) Science Journal, June 2013, Pages 396-399.